Available online at www.sciencedirect.com
SCIENCE DIRECT®
Nuclear Physics A 735 (2004) 393–424
NUCLEAR PHYSICS A
www.elsevier.com/locate/npe

Coexisting normal and triaxial superdeformed structures in ^{165}Lu

G. Schönwaßer [a], N. Nenoff [a], H. Hübel [a,*], G.B. Hagemann [b], P. Bednarczyk [c,d], G. Benzoni [e], A. Bracco [e], P. Bringel [a], R. Chapman [f], D. Curien [c], J. Domscheit [a], B. Herskind [b], D.R. Jensen [b], S. Leoni [e], G. Lo Bianco [g], W.C. Ma [h], A. Maj [d], A. Neußer [a], S.W. Ødegård [i], C.M. Petrache [g], D. Roßbach [a], H. Ryde [j], A.K. Singh [a], K.H. Spohr [f]

[a] *Helmholtz-Institut für Strahlen- und Kernphysik, Universität Bonn, Nussallee 14-16, D-53115 Bonn, Germany*
[b] *The Niels Bohr Institute, Blegdamsvej 17, DK-2100 Copenhagen Ø, Denmark*
[c] *Institut de Recherches Subatomiques, F-67037 Strasbourg cedex 2, France*
[d] *Niewodniczanski Institute of Nuclear Physics, Polish Academy of Sciences, Krakow, Poland*
[e] *Dipartimento di Fisica and INFN, Sezione di Milano, Università di Milano, I-20133 Milano, Italy*
[f] *Department of Electronic Engineering and Physics, University of Paisley, Paisley PA1 28E, UK*
[g] *Dipartimento di Fisica and INFN, Sezione di Perugia, Università di Camerino, I-62032 Camerino, Italy*
[h] *Mississippi State University, Mississippi State, MS 39762, USA*
[i] *Department of Physics, University of Oslo, N-0316 Oslo, Norway*
[j] *Department of Physics, University of Lund, S-22362 Lund, Sweden*

Received 14 January 2004; received in revised form 4 February 2004; accepted 6 February 2004

Abstract

High-spin states in ^{165}Lu were populated in the ^{139}La(^{30}Si, $4n$) reaction at a beam energy of 152 MeV and γ-ray coincidences were measured with the EUROBALL spectrometer array. Nine new rotational bands were discovered, known band structures were considerably extended and many inter-band transitions were found. Structures with normal deformation coexist with bands associated with the strongly deformed triaxial energy minima found in calculations. Three of these triaxial bands form a family of wobbling excitations with phonon quanta $n_w = 0$, 1 and 2. The wobbling mode is a unique signature of nuclear triaxiality. Configuration assignments are discussed for the observed band

* Corresponding author.
E-mail address: hubel@iskp.uni-bonn.de (H. Hübel).

0375-9474/$ – see front matter © 2004 Elsevier B.V. All rights reserved.
doi:10.1016/j.nuclphysa.2004.02.006

structures. An exchange of configuration between two of the new bands due to mixing is observed, resulting in different signature partnerships at low and high spins.
© 2004 Elsevier B.V. All rights reserved.

PACS: 21.10.-k; 21.10.Re; 23.20.Lv; 27.70.+q

Keywords: NUCLEAR REACTIONS ^{139}La(^{30}Si, 4n), $E = 152$ MeV; measured E_γ, I_γ, $\gamma\gamma$-coin. ^{165}Lu deduced high-spin levels, J, π, configurations, shape coexistence, triaxial deformation. Euroball array

1. Introduction

High-spin spectroscopic studies of nuclei in the mass region around $A = 165$ have established that normal-deformed (ND) structures coexist with triaxial superdeformed (TSD) shapes [1–20]. Shape coexistence in these nuclei had been predicted theoretically more than 10 years ago [21,22]. When the first TSD bands were found experimentally, it was suggested [1–3] that the strongly deformation-driving proton $i_{13/2}$ orbital is involved in the configuration of the TSD structures. More recent calculations of total-energy surfaces with the ultimate cranker (UC) code [23], based on a deformed harmonic oscillator potential, also predict local minima at normal deformation, around $\epsilon_2 = 0.2$, coexisting with minima at $\epsilon_2 \approx 0.4$ with a pronounced triaxiality of $\gamma \approx \pm 20°$. In Fig. 1 an example of such calculations is shown for ^{165}Lu for a spin of $61/2$ and for parity and signature $(+, +1/2)$. The TSD minima are predicted for all combinations of parity and signature. They result from a shell gap at $Z = 72$ and $N = 94$ for large triaxiality [3]. In general, in the calculations the local minima with positive triaxiality parameters γ have lower energy than the minima with negative values of γ.

Lifetimes have been measured for several of the yrast TSD bands in this mass region [2,9,13–15] from which transition quadrupole moments have been derived. They are found to be substantially larger than those of the ND bands. In all the observed bands the dynamic moments of inertia are similar, and larger than those of the ND structures.

Experimentally, a deviation from axial symmetry is difficult to prove. A unique signature of triaxiality is the occurrence of wobbling bands which were predicted more than 25 years ago [24]. Nuclear wobbling was discovered only recently in ^{163}Lu [10–12], ^{165}Lu [16] and ^{167}Lu [19]. The presence of the aligned $i_{13/2}$ proton favours the triaxial shape and results in a unique pattern of transition strengths between the wobbling bands [25,26]. The comparison of these properties with theoretical expectations for the wobbling motion provided the evidence for this mode of excitation in the three Lu isotopes.

In the present work, we report on the results of an experiment to study the high-spin structure of ^{165}Lu carried out with the EUROBALL γ-ray spectrometer array [27]. Our results for the three wobbling TSD bands in this nucleus with wobbling phonon numbers $n_w = 0$, 1 and 2 have been published previously [16]. Thus, the emphasis of this paper is on the ND structures and the properties of the TSD bands are only briefly reviewed, including two new weakly populated TSD bands. The previously known level scheme of ^{165}Lu [3–5] is appreciably extended. Nine new bands have been discovered, known bands have been extended to higher spin and many new inter-band transitions have been established.

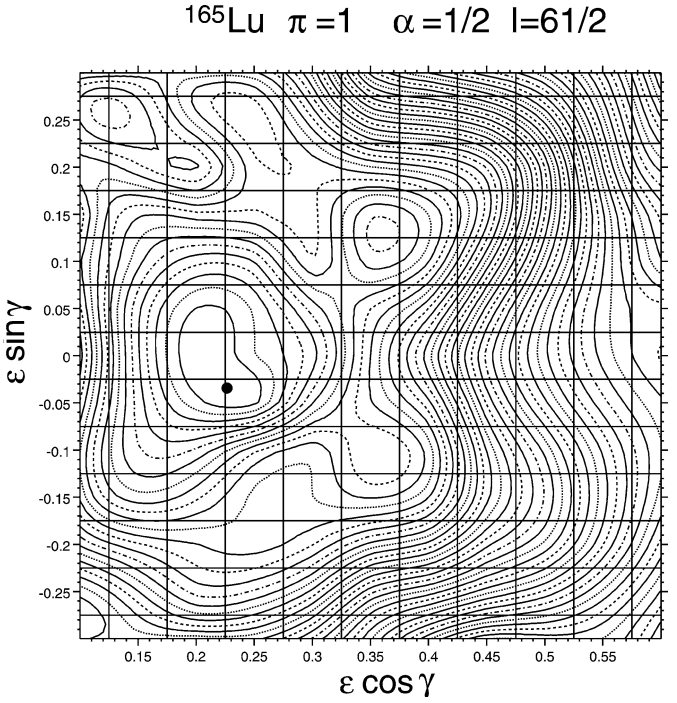

Fig. 1. Example of the potential-energy surfaces calculated with the Ultimate Cranker code [23] for positive parity, signature $+1/2$ and spin $61/2$ for ^{165}Lu.

The experimental details are outlined in section two, followed by a presentation of the results. In section three the configuration assignments to the bands as well as the origin of the observed band crossings are discussed. The last section gives a short summary.

2. Experimental details and results

High-spin states in ^{165}Lu were populated in the reaction ^{139}La(^{30}Si, $4n$). The ^{30}Si beam of 152 MeV was provided by the Vivitron Tandem accelerator at IReS, Strasbourg. Two ^{139}La foils, each of 500 μg/cm^2 thickness, were used as target. The target foils were produced a few days before the experiment and handled in an Argon atmosphere to prevent oxidation.

Gamma-ray coincidences were measured with the EUROBALL spectrometer array [27]. It comprises 30 conventional large-volume tapered Ge detectors as well as 26 Clover and 15 Cluster composite Ge detectors. The Clover detectors consist of four Ge crystals each and the Clusters are composed of seven crystals each. Out of the maximum total of 239 Ge crystals, ten were rejected during the presorting of the data because they showed instabilities that could not be recovered by the gain-matching routines. All detectors are surrounded by bismuth germanate (BGO) scintillation detectors for Compton suppression.

In addition, an inner ball of 210 BGO detectors was used as a multiplicity filter to enhance the detection of high-spin states which deexcite in long γ-ray cascades.

Coincidence events were written to magnetic tape when five or more γ-rays were detected in the Ge crystals before Compton suppression and ten or more γ-rays were detected in the BGO detectors of the inner ball. After gain-matching and presorting a total of 3.2×10^9 three- and higher-fold Compton-suppressed coincidence events remained for further analysis. These events were sorted into a three-dimensional array (3D Radware cube [28]) and into a BLUE [29] data base. The BLUE data base allows for an easy access to coincidence spectra and for the analysis of γ-ray directional correlations from the nuclei oriented in the reaction (DCO ratios).

Examples of the γ-ray coincidence spectra are shown in Figs. 2–5. Figs. 2 and 3 show spectra of ND bands which were partly known [3–5] before our work. Our data allow us to extend these bands to higher spins and to identify further transitions in their decay towards the ground state of ^{165}Lu. In Fig. 4 spectra of a number of new bands are displayed. They are in coincidence with known transitions in ^{165}Lu which makes their assignment to this nucleus unambiguous. Finally, Fig. 5 shows the spectra of the five TSD bands. Bands TSD 1–3, which form the family of wobbling bands with phonon numbers $n_w = 0$, 1 and 2, have been discussed in our recent publication [16]. The bands TSD 4 and TSD 5 could not be linked to the main level scheme and their decay paths are not clear. For band N1 only one tentative link was found.

Gamma-ray transition energies, relative intensities, DCO ratios and spin assignments to excited states in ^{165}Lu are summarized in Table 1. The transitions are grouped according to the bands shown in the energy-level schemes displayed in Figs. 6 and 7. Inter-band and decay-out transitions are listed together with the bands from which they originate. The fitting routine within the Radware software [28] package was used to determine the γ-ray intensities. The intensities of the strongest transitions were determined in the total-projection spectrum. For weaker transitions and unresolved lines the intensities were determined in coincidence spectra with proper normalization. For the multipolarity assignments given in the table, E2 was assumed when the DCO ratios are compatible with stretched quadrupoles. In the cases where DCO ratios compatible with stretched dipole multipole order were found, E1 or M1 are possible. However, the complex decay pattern and the observed inter-band transitions allowed unambiguous multipolarity assignments. For the M1 transitions, E2 admixtures cannot be ruled out. In several cases the DCO ratios for E2 transitions near the bottom of a band are smaller than unity. This might be due to a loss of spin alignment by relaxation effects if the levels have lifetimes.

The level scheme of the ND band structures in ^{165}Lu is displayed in Fig. 6. Fig. 7 shows the partial level scheme of the TSD bands, including the two new shorter sequences TSD 4 and 5. The level schemes have been constructed on the basis of the γ-ray coincidence data and intensity balances. The widths of the arrows are proportional to the observed γ-ray intensities. Large parts of the ND level structure and of TSD band 1 are in agreement with previous work [3–5], but parts of the previously known level scheme had to be revised and all the bands have been extended to higher spins. Experimental details for TSD 1 to 3 have already been presented in our earlier paper [16].

In the following, we comment on some details of the ND level scheme and explain the spin-parity assignments for the new bands.

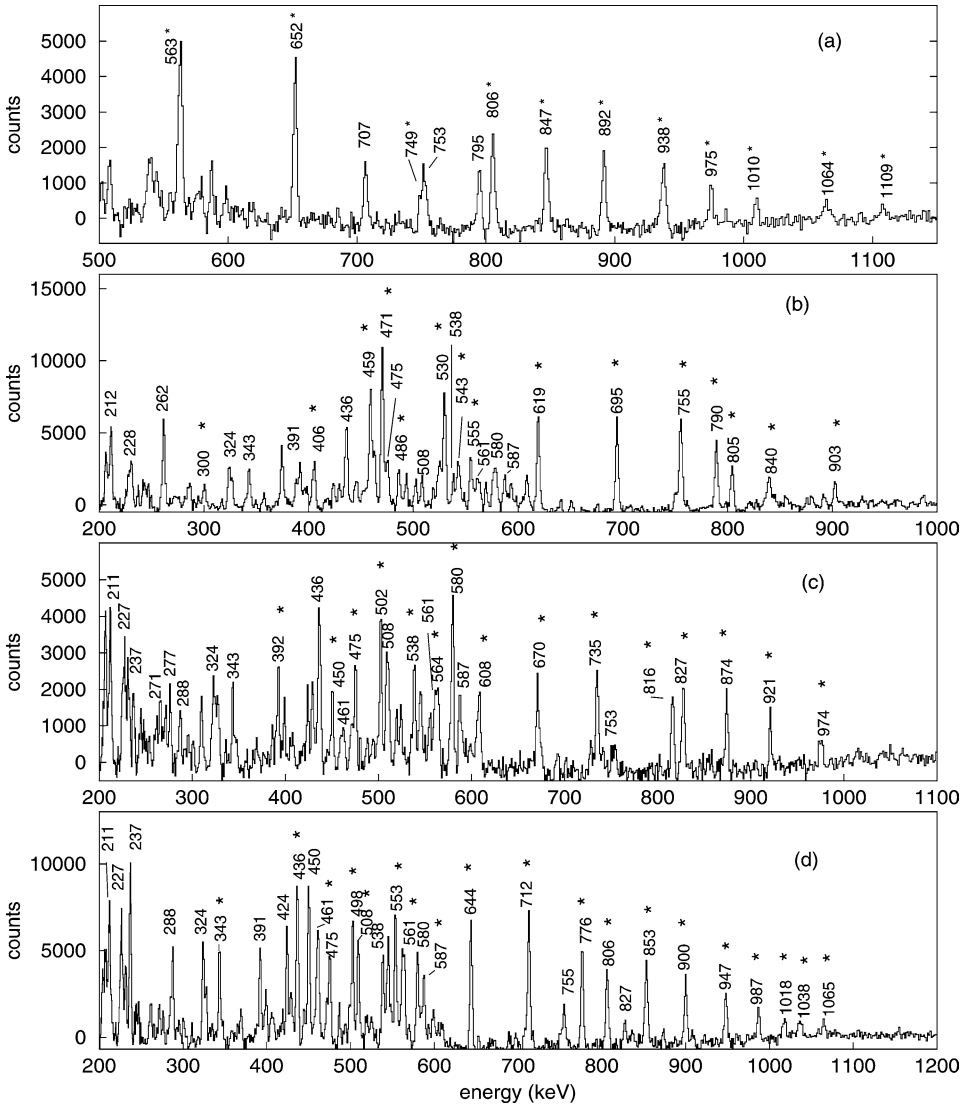

Fig. 2. Gamma-ray coincidence spectra of positive-parity bands in ^{165}Lu: (a) [411]1/2 $\alpha = -1/2$, (b) [402]5/2 $\alpha = +1/2$, (c) [404]7/2 $\alpha = +1/2$ and (d) [404]7/2 $\alpha = -1/2$. Gates were set on transitions between high-spin states to highlight the extensions of the bands. Band members are marked by asterisks.

The new band labelled N1 in Fig. 6 consists of five levels. It decays into the [541]1/2$^-$ band. We tentatively assign the 716 keV transition as one of the linking transitions. The suggested spin and parity are not firmly established.

The previously known [541]1/2$^-$ decoupled band [3–5] has been extended by ten states up to spin 77/2$^-$. This allows the identification of a second band crossing in this band at $\hbar\omega \approx 0.48$ MeV.

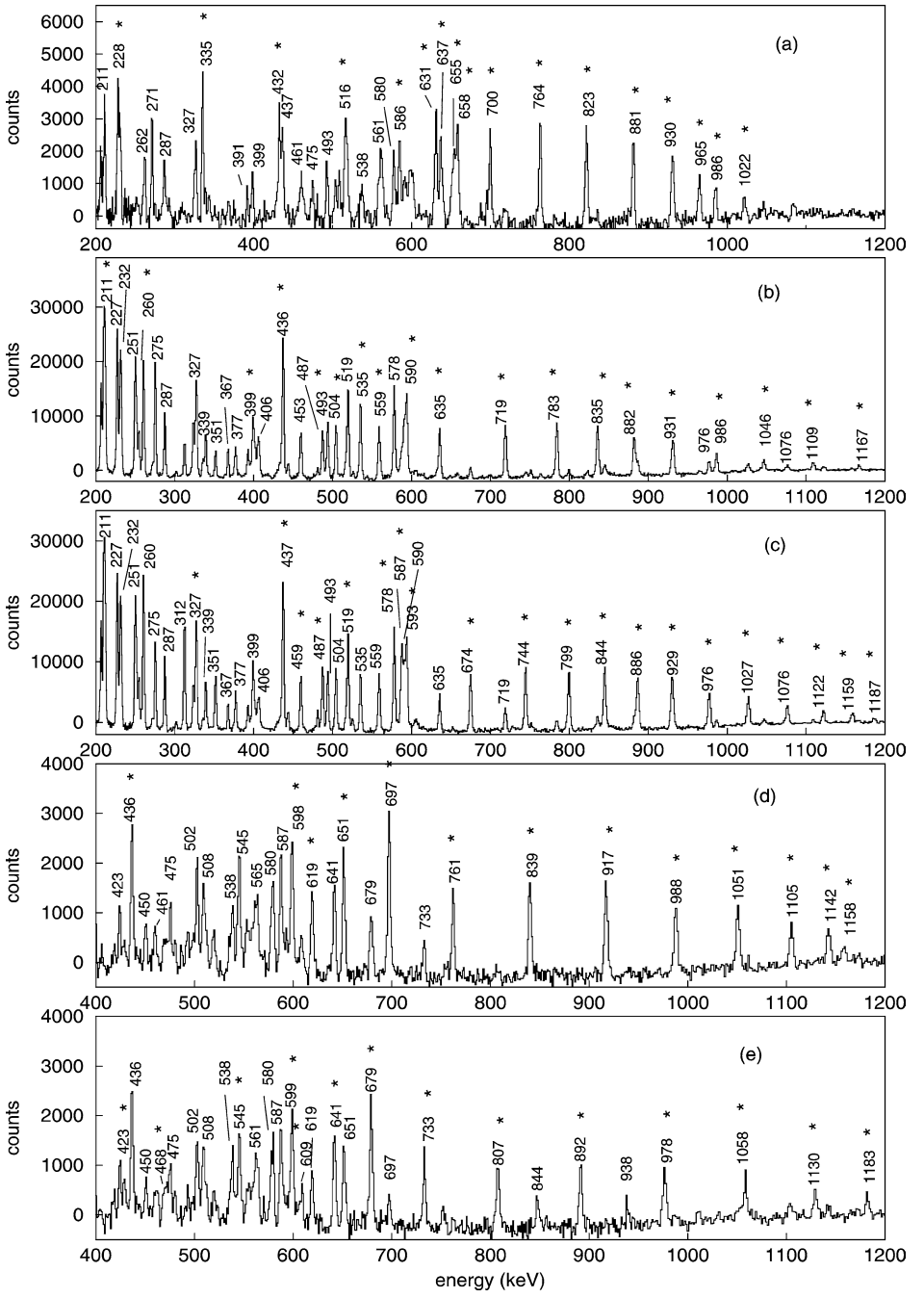

Fig. 3. Gamma-ray coincidence spectra of bands in ^{165}Lu: (a) [541]1/2, (b) [514]9/2 $\alpha = +1/2$, (c) [514]9/2 $\alpha = -1/2$, (d) [514]9/2$\otimes$AE $\alpha = +1/2$ and (e) [514]9/2$\otimes$AE $\alpha = -1/2$. Gates were set on transitions between high-spin states to highlight the extensions of the bands. Band members are marked by asterisks.

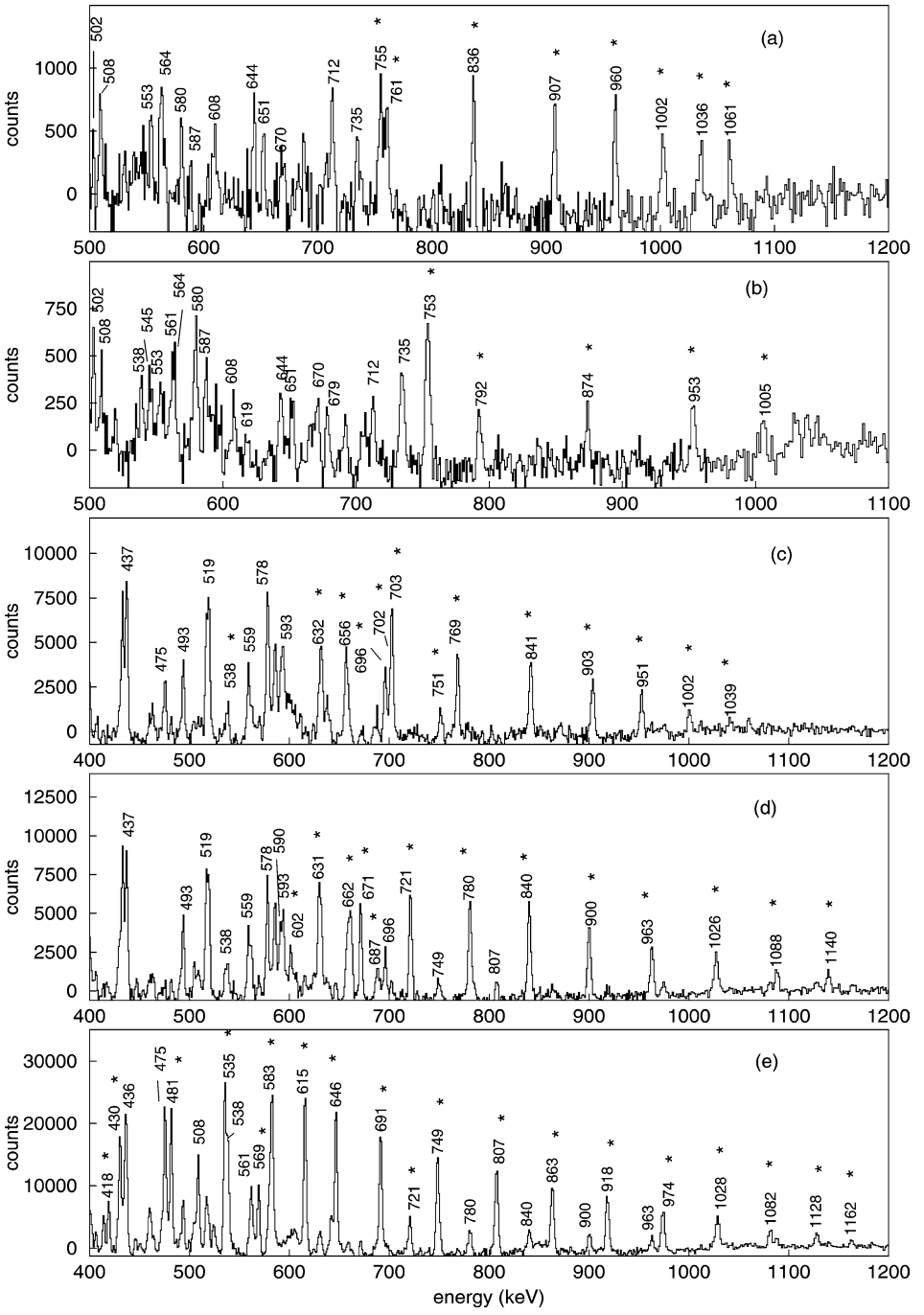

Fig. 4. Gamma-ray coincidence spectra of new ND bands in ^{165}Lu. In the level scheme presented in Fig. 6, they are labelled (a) N2, (b) N3, (c) N5, (d) N6 and (e) N7. The band members are marked by asterisks.

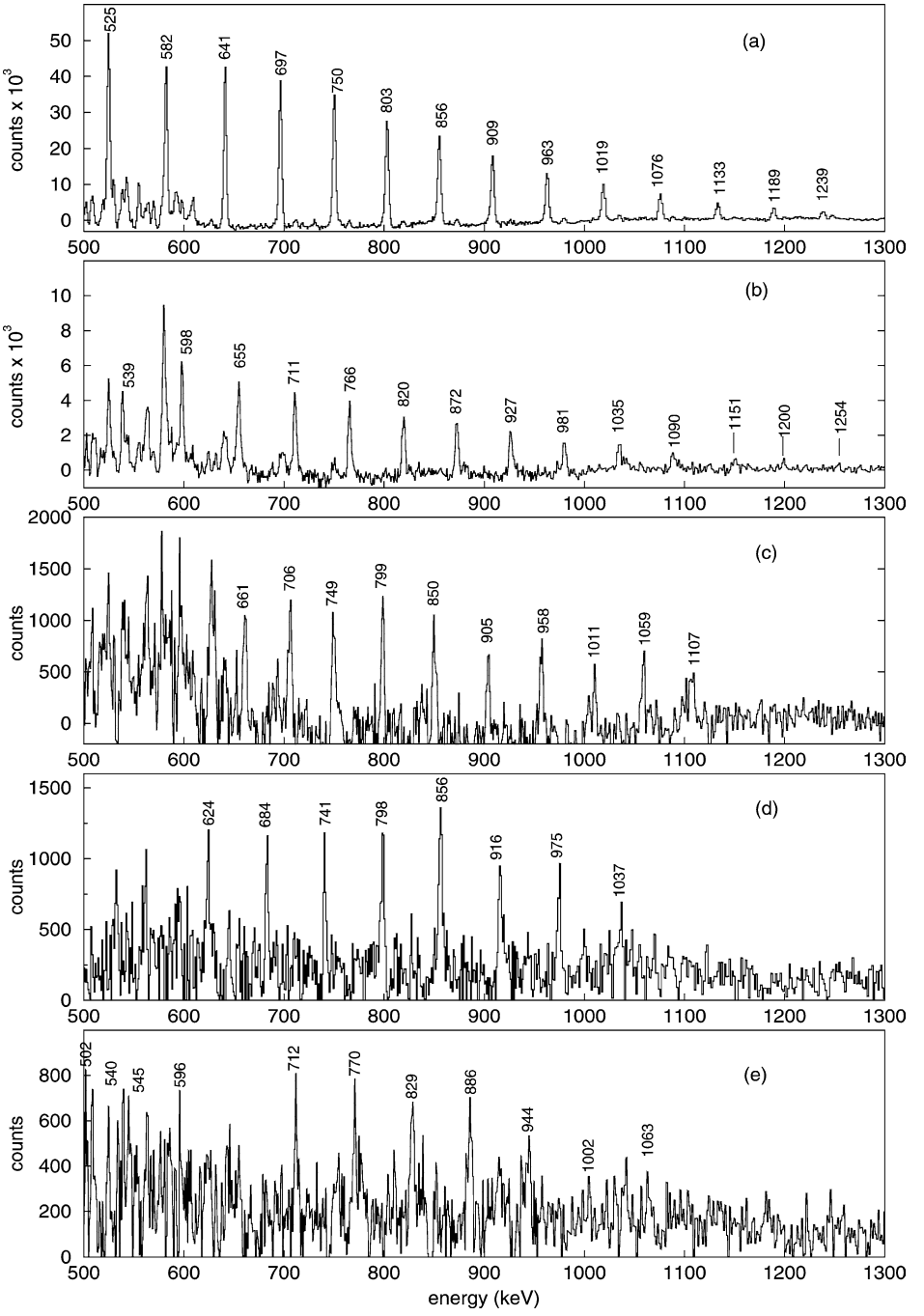

Fig. 5. Gamma-ray coincidence spectra of TSD bands in ^{165}Lu. In the level scheme of Fig. 7 they are labelled (a) TSD 1, (b) TSD 2, (c) TSD 3, (d) TSD 4 and (e) TSD 5.

Table 1
Energies, intensities, DCO ratios, spin assignments and multipolarity of γ-ray transitions observed in ^{165}Lu

Energy[a] E_γ (keV)	Intensity[b] I_γ (rel.)	R_{DCO}[c] $I_\gamma(25°)/I_\gamma(90°)$	Multip.	Excitation E_i (keV)	Assignment $J_i^\pi \to J_f^\pi$
		[514]9/2$^-$ band			
93.6	–	–	E1	235	$9/2^- \to 7/2^+$
180.2	108	0.60(6)	(M1)	235	$9/2^- \to (7/2^-)$
211.5	119	0.60(6)	E1	235	$9/2^- \to 7/2^+$
159.4	88	0.55(6)	M1	495	$13/2^- \to 11/2^-$
259.8	65	–[d]	E2	495	$13/2^- \to 9/2^-$
230.7	86	0.61(7)	M1	893	$17/2^- \to 15/2^-$
398.6	60	0.92(8)	E2	893	$17/2^- \to 13/2^-$
287.0	62	0.67(7)	M1	1387	$21/2^- \to 19/2^-$
493.1	61	1.05(9)	E2	1387	$21/2^- \to 17/2^-$
326.6	43	–[d]	M1	1945	$25/2^- \to 23/2^-$
558.5	57	1.02(9)	E2	1945	$25/2^- \to 21/2^-$
338.9	32	0.65(6)	M1	2535	$29/2^- \to 27/2^-$
589.8	56	1.03(9)	E2	2535	$29/2^- \to 25/2^-$
249.7	50	0.56(6)	M1	3039	$33/2^- \to 31/2^-$
503.7	40	1.08(11)	E2	3039	$33/2^- \to 29/2^-$
226.8	59	0.56(6)	M1	3475	$37/2^- \to 35/2^-$
436.4	23.8	0.94(9)	E2	3475	$37/2^- \to 33/2^-$
275.0	34	0.61(7)	M1	4010	$41/2^- \to 39/2^-$
535.1	32	1.04(9)	E2	4010	$41/2^- \to 37/2^-$
322.7	22.2	0.69(8)	M1	4645	$45/2^- \to 43/2^-$
635.2	26.3	1.06(9)	E2	4645	$45/2^- \to 41/2^-$
367.2	10.9	0.61(6)	M1	5364	$49/2^- \to 47/2^-$
718.7	23.8	1.00(11)	E2	5364	$49/2^- \to 45/2^-$
406.0	7.8	0.65(8)	M1	6147	$53/2^- \to 51/2^-$
783.3	16.9	1.04(11)	E2	6147	$53/2^- \to 49/2^-$
442.9	4.2	0.52(7)	M1	6983	$57/2^- \to 55/2^-$
835.4	15.4	0.91(9)	E2	6983	$57/2^- \to 53/2^-$
881.6	9.2	1.20(12)	E2	7864	$61/2^- \to 57/2^-$
931.0	6.7	1.16(12)	E2	8795	$65/2^- \to 61/2^-$
986.0	3.4	1.08(11)	E2	9781	$69/2^- \to 65/2^-$
1046.0	2.2	–	E2	10827	$73/2^- \to 69/2^-$
1108.9	1.4	–	E2	11936	$77/2^- \to 73/2^-$
1166.5	0.6	–	E2	13103	$81/2^- \to 77/2^-$
100.6	12	0.48(6)	M1	335	$11/2^- \to 9/2^-$
152.7	1.2	0.5(1)	E1	335	$11/2^- \to 9/2^+$
168.2	77	0.58(6)	M1	663	$15/2^- \to 13/2^-$
327.0	57	–[d]	E2	663	$15/2^- \to 11/2^-$
206.4	72	0.68(6)	M1	1100	$19/2^- \to 17/2^-$
436.6	97	0.94(7)	E2	1100	$19/2^- \to 15/2^-$
232.1	43	0.71(8)	M1	1619	$23/2^- \to 21/2^-$
518.8	100	1.06(8)	E2	1619	$23/2^- \to 19/2^-$
251.0	27.9	0.64(6)	M1	2196	$27/2^- \to 25/2^-$
577.6	97	1.06(9)	E2	2196	$27/2^- \to 23/2^-$
254.1	27.2	0.60(6)	M1	2789	$31/2^- \to 29/2^-$
593.2	86	0.90(9)	E2	2789	$31/2^- \to 27/2^-$
209.7	64	0.60(7)	M1	3249	$35/2^- \to 33/2^-$

(*continued on next page*)

Table 1 (*continued*)

Energy[a] E_γ (keV)	Intensity[b] I_γ (rel.)	R_{DCO}[c] $I_\gamma(25°)/I_\gamma(90°)$	Multip.	Excitation E_i (keV)	Assignment $J_i^\pi \to J_f^\pi$
301.1	1.2	–	E2	3249	$35/2^- \to 31/2^-$
459.1	28.1	1.08(9)	E2	3249	$35/2^- \to 31/2^-$
260.0	43	–[d]	M1	3735	$39/2^- \to 37/2^-$
486.6	22.7	1.02(9)	E2	3735	$39/2^- \to 35/2^-$
312.0	27.3	0.56(6)	M1	4322	$43/2^- \to 41/2^-$
586.8	22.1	1.16(11)	E2	4322	$43/2^- \to 39/2^-$
351.2	13.7	0.55(6)	M1	4997	$47/2^- \to 45/2^-$
674.1	20.3	1.02(9)	E2	4997	$47/2^- \to 43/2^-$
377.0	8.6	0.58(7)	M1	5741	$51/2^- \to 49/2^-$
743.9	17.0	1.00(9)	E2	5741	$51/2^- \to 47/2^-$
391.8	5.1	0.72(9)	M1	6539	$55/2^- \to 53/2^-$
798.7	12.5	1.02(11)	E2	6539	$55/2^- \to 51/2^-$
401.2	3.9	–	M1	7384	$59/2^- \to 57/2^-$
844.5	11.0	0.89(9)	E2	7384	$59/2^- \to 55/2^-$
405.0	3.2	0.65(7)	M1	8270	$63/2^- \to 61/2^-$
886.2	9.3	1.15(11)	E2	8270	$63/2^- \to 59/2^-$
929.4	5.0	1.08(9)	E2	9199	$67/2^- \to 63/2^-$
976.4	3.8	1.06(9)	E2	10176	$71/2^- \to 67/2^-$
1026.6	3.0	1.14(12)	E2	11202	$75/2^- \to 71/2^-$
1076.0	2.4	0.89(13)	E2	12278	$79/2^- \to 75/2^-$
1121.7	1.4	1.11(14)	E2	13400	$83/2^- \to 79/2^-$
1158.8	0.7	–	E2	14559	$87/2^- \to 83/2^-$
1187.0	0.40	–	E2	15746	$91/2^- \to 87/2^-$
			[404]7/2$^+$ band		
184.3	28.4	0.61(7)	M1	367	$11/2^+ \to 9/2^+$
343.0	34.3	0.93(9)	E2	367	$11/2^+ \to 7/2^+$
228.2	14.6	0.80(11)	M1	802	$15/2^+ \to 13/2^+$
435.6	47.1	0.95(9)	E2	802	$15/2^+ \to 11/2^+$
262.0	9.1	0.65(7)	M1	1311	$19/2^+ \to 17/2^+$
508.4	50.7	1.14(12)	E2	1311	$19/2^+ \to 15/2^+$
284.5	5.6	0.64(8)	M1	1872	$23/2^+ \to 21/2^+$
561.0	42.4	0.98(9)	E2	1872	$23/2^+ \to 19/2^+$
291.8	6.6	0.75(12)	M1	2459	$27/2^+ \to 25/2^+$
587.0	36.9	1.10(9)	E2	2459	$27/2^+ \to 23/2^+$
226.5	14.2	0.64(8)	M1	2957	$31/2^+ \to 29/2^+$
418.1	7.0	1.01(11)	E2	2957	$31/2^+ \to 27/2^+$
498.3	6.7	1.05(11)	E2	2957	$31/2^+ \to 27/2^+$
214.1	1.2	–	M1	3417	$35/2^+ \to 33/2^+$
237.2	10.7	0.53(8)	M1	3417	$35/2^+ \to 33/2^+$
449.0	7.1	1.02(9)	E2	3417	$35/2^+ \to 31/2^+$
460.5	10.7	0.89(11)	E2	3417	$35/2^+ \to 31/2^+$
287.6	5.1	0.58(7)	M1	3970	$39/2^+ \to 37/2^+$
552.9	10.0	1.01(11)	E2	3970	$39/2^+ \to 35/2^+$
643.7	10.4	1.13(12)	E2	4614	$43/2^+ \to 39/2^+$
712.0	7.2	1.09(11)	E2	5326	$47/2^+ \to 43/2^+$
708.1	0.6	–	E2	6102	$51/2^+ \to 47/2^+$
775.8	4.3	1.21(15)	E2	6102	$51/2^+ \to 47/2^+$

(*continued*)

Table 1 (*continued*)

Energy[a] E_γ (keV)	Intensity[b] I_γ (rel.)	R_{DCO}[c] $I_\gamma(25°)/I_\gamma(90°)$	Multip.	Excitation E_i (keV)	Assignment $J_i^\pi \to J_f^\pi$
805.9	2.6	1.20(16)	E2	6908	$55/2^+ \to 51/2^+$
826.7	0.2	–	E2	6908	$55/2^+ \to 51/2^+$
852.7	2.3	–	E2	7760	$59/2^+ \to 55/2^+$
900.1	2.2	–	E2	8660	$63/2^+ \to 59/2^+$
946.7	1.6	–	E2	9607	$67/2^+ \to 63/2^+$
986.9	1.3	–	E2	10594	$71/2^+ \to 67/2^+$
1018.2	1.0	–	E2	11612	$75/2^+ \to 71/2^+$
1037.7	0.9	–	E2	12650	$79/2^+ \to 75/2^+$
1065.0	0.5	–	E2	13715	$83/2^+ \to 79/2^+$
159.2	57	0.64(7)	M1	182	$9/2^+ \to 7/2^+$
207.6	23.0	0.73(9)	M1	574	$13/2^+ \to 11/2^+$
391.7	45.3	0.89(9)	E2	574	$13/2^+ \to 9/2^+$
246.7	10.8	0.72(9)	M1	1049	$17/2^+ \to 15/2^+$
474.7	51.0	1.01(9)	E2	1049	$17/2^+ \to 13/2^+$
276.5	13.4	0.50(7)	M1	1587	$21/2^+ \to 19/2^+$
538.2	52	1.03(9)	E2	1587	$21/2^+ \to 17/2^+$
295.0	9.6	0.65(9)	M1	2167	$25/2^+ \to 23/2^+$
579.7	53	1.04(9)	E2	2167	$25/2^+ \to 21/2^+$
271.4	13.1	0.48(7)	M1	2730	$29/2^+ \to 27/2^+$
563.6	27.9	1.04(9)	E2	2730	$29/2^+ \to 25/2^+$
224.3	8.4	–[d]	M1	3180	$33/2^+ \to 31/2^+$
450.1	7.0	1.06(11)	E2	3180	$33/2^+ \to 29/2^+$
265.3	8.7	0.50(9)	M1	3683	$37/2^+ \to 35/2^+$
502.0	6.3	1.02(11)	E2	3683	$37/2^+ \to 33/2^+$
309.4	2.2	–	M1	4291	$41/2^+ \to 39/2^+$
608.0	8.6	0.89(11)	E2	4291	$41/2^+ \to 37/2^+$
346.6	2.8	–	M1	4961	$45/2^+ \to 43/2^+$
690.5	2.0	–	E2	4961	$45/2^+ \to 41/2^+$
670.0	4.7	1.20(15)	E2	4961	$45/2^+ \to 41/2^+$
735.0	4.1	0.98(15)	E2	5696	$49/2^+ \to 45/2^+$
816.0	2.3	1.19(16)	E2	6511	$53/2^+ \to 49/2^+$
827.0	1.7	1.05(16)	E2	7338	$57/2^+ \to 53/2^+$
874.0	1.3	1.06(16)	E2	8212	$61/2^+ \to 57/2^+$
921.0	1.2	–	E2	9133	$65/2^+ \to 61/2^+$
974.0	0.60	–	E2	10107	$69/2^+ \to 65/2^+$
		[411]$1/2^+$ band			
48.0	–	–	M1	195	$7/2^+ \to 5/2^+$
195.4	63	0.65(7)	E2	195	$7/2^+ \to 3/2^+$
214.1	3.8	–	M1	520	$11/2^+ \to 9/2^+$
324.2	29	0.92(8)	E2	520	$11/2^+ \to 7/2^+$
231.9	6.5	0.70(6)	M1	943	$15/2^+ \to 13/2^+$
423.7	19.0	1.06(9)	E2	943	$15/2^+ \to 11/2^+$
444.1	9.2	1.31(21)	E2	943	$15/2^+ \to 11/2^+$
502.1	30	1.23(13)	E2	1445	$19/2^+ \to 15/2^+$
544.7	30	1.20(12)	E2	1990	$23/2^+ \to 19/2^+$
548.4	14.2	1.05(12)	E2	2539	$27/2^+ \to 23/2^+$
269.4	1.7	0.6(1)	M1	3000	$31/2^+ \to 29/2^+$

(*continued on next page*)

Table 1 (*continued*)

Energy[a] E_γ (keV)	Intensity[b] I_γ (rel.)	R_{DCO}[c] $I_\gamma(25°)/I_\gamma(90°)$	Multip.	Excitation E_i (keV)	Assignment $J_i^\pi \to J_f^\pi$
455.0	1.2	1.15(21)	E2	3000	$31/2^+ \to 27/2^+$
461.0	1.9	1.20(22)	E2	3000	$31/2^+ \to 27/2^+$
540.9	3.8	1.05(11)	E2	3000	$31/2^+ \to 27/2^+$
472.0	9.6	1.12(11)	E2	3472	$35/2^+ \to 31/2^+$
563.0	8.8	1.12(12)	E2	4035	$39/2^+ \to 35/2^+$
652.0	8.4	1.02(11)	E2	4687	$43/2^+ \to 39/2^+$
749.0	1.80	1.14(20)	E2	5436	$47/2^+ \to 43/2^+$
707.0	5.1	0.98(9)	E2	5394	$47/2^+ \to 43/2^+$
753.0	1.3	1.05(22)	E2	6189	$51/2^+ \to 47/2^+$
795.0	0.9	1.15(18)	E2	6189	$51/2^+ \to 47/2^+$
806.0	1.9	1.05(18)	E2	6995	$55/2^+ \to 51/2^+$
847.0	1.4	0.95(15)	E2	7842	$59/2^+ \to 55/2^+$
892.0	1.3	0.98(17)	E2	8734	$63/2^+ \to 59/2^+$
938.0	1.2	–	E2	9672	$67/2^+ \to 63/2^+$
975.0	1.0	–	E2	10647	$71/2^+ \to 67/2^+$
1010.0	0.8	–	E2	11657	$75/2^+ \to 71/2^+$
1064.0	0.5	–	E2	12721	$79/2^+ \to 75/2^+$
1109.0	0.4	–	E2	13830	$83/2^+ \to 79/2^+$
147.7	5.8	0.52(6)	M1	148	$5/2^+ \to 3/2^+$
237.4	4.9	0.63(6)	M1	433	$9/2^+ \to 7/2^+$
285.0	6.0	0.80(7)	E2	433	$9/2^+ \to 5/2^+$
301.5	4.4	0.48(6)	M1	821	$13/2^+ \to 11/2^+$
388.5	12.3	0.93(7)	E2	821	$13/2^+ \to 9/2^+$
348.3	2.0	–	M1	1292	$17/2^+ \to 15/2^+$
470.9	9.9	1.04(8)	E2	1292	$17/2^+ \to 13/2^+$
373.0	2.4	–	M1	1818	$21/2^+ \to 19/2^+$
526.1	9.4	1.10(8)	E2	1818	$21/2^+ \to 17/2^+$
530.2	4.3	1.05(11)	E2	2349	$25/2^+ \to 21/2^+$
608.8	7.3	1.10(12)	E2	2349	$25/2^+ \to 21/2^+$
		[541]$1/2^-$ band			
345.5	3.2	–	E1	346	$5/2^- \to 3/2^+$
121.1	1.2	–	E2	467	$9/2^- \to 5/2^-$
271.1	27.9	0.59(6)	E1	467	$9/2^- \to 7/2^+$
175.1	4.9	0.4(1)	E1	695	$13/2^- \to 11/2^+$
228.3	28.8	0.64(6)	E2	695	$13/2^- \to 9/2^-$
335.4	37.9	0.80(6)	E2	1030	$17/2^- \to 13/2^-$
432.1	32.4	1.00(6)	E2	1462	$21/2^- \to 17/2^-$
516.4	28.9	1.04(8)	E2	1979	$25/2^- \to 21/2^-$
585.7	22.1	1.17(9)	E2	2564	$29/2^- \to 25/2^-$
630.9	13.2	1.14(9)	E2	3195	$33/2^- \to 29/2^-$
658.4	8.9	1.05(10)	E2	3854	$37/2^- \to 33/2^-$
637.1	5.3	1.10(12)	E2	4491	$41/2^- \to 37/2^-$
654.5	3.1	0.93(12)	E2	5145	$45/2^- \to 41/2^-$
700.0	2.6	0.90(11)	E2	5845	$49/2^- \to 45/2^-$
763.5	1.4	1.05(11)	E2	6609	$53/2^- \to 49/2^-$
822.6	1.3	1.10(12)	E2	7431	$57/2^- \to 53/2^-$
881.0	1.2	1.06(12)	E2	8312	$61/2^- \to 57/2^-$

(*continued*)

Table 1 (*continued*)

Energy[a] E_γ (keV)	Intensity[b] I_γ (rel.)	R_{DCO}[c] $I_\gamma(25°)/I_\gamma(90°)$	Multip.	Excitation E_i (keV)	Assignment $J_i^\pi \to J_f^\pi$
930.2	0.8	–	E2	9243	$65/2^- \to 61/2^-$
965.1	0.6	–	E2	10208	$69/2^- \to 65/2^-$
986.4	0.4	–	E2	11194	$73/2^- \to 69/2^-$
1021.7	0.2	–	E2	12216	$77/2^- \to 73/2^-$
		[402]$5/2^+$ band			
164.3	11.1	0.57(6)	M1	305	$9/2^+ \to 7/2^+$
300.1	3.4	0.85(14)	E2	305	$9/2^+ \to 5/2^+$
191.6	2.4	–	M1	711	$13/2^+ \to 11/2^+$
212.2	10.4	0.46(6)	M1	711	$13/2^+ \to 11/2^+$
344.8	3.8	–[d]	M1	711	$13/2^+ \to 11/2^+$
405.6	7.3	0.91(9)	E2	711	$13/2^+ \to 9/2^+$
241.8	6.6	0.58(6)	M1	1197	$17/2^+ \to 15/2^+$
486.1	10.0	0.99(9)	E2	1197	$17/2^+ \to 13/2^+$
262.0	5.9	0.54(6)	M1	1740	$21/2^+ \to 19/2^+$
448.6	0.3	–	E2	1740	$21/2^+ \to 17/2^+$
542.6	10.8	1.02(9)	E2	1740	$21/2^+ \to 17/2^+$
246.3	1.3	–	M1	2294	$25/2^+ \to 23/2^+$
475.0	2.6	0.95(11)	E2	2294	$25/2^+ \to 21/2^+$
554.6	9.7	1.08(9)	E2	2294	$25/2^+ \to 21/2^+$
404.8	3.9	–[d]	E2	2753	$29/2^+ \to 25/2^+$
459.0	12.6	1.01(9)	E2	2753	$29/2^+ \to 25/2^+$
471.0	6.8	0.95(9)	E2	3224	$33/2^+ \to 29/2^+$
530.1	5.7	1.09(9)	E2	3755	$37/2^+ \to 33/2^+$
608.8	1.9	–	E2	4374	$41/2^+ \to 37/2^+$
619.4	5.6	0.91(9)	E2	4374	$41/2^+ \to 37/2^+$
694.8	3.3	0.89(9)	E2	5069	$45/2^+ \to 41/2^+$
755.0	3.0	0.93(9)	E2	5824	$49/2^+ \to 45/2^+$
789.5	2.0	1.04(11)	E2	6613	$53/2^+ \to 49/2^+$
804.9	1.4	–	E2	7418	$57/2^+ \to 53/2^+$
839.8	0.8	–	E2	8258	$61/2^+ \to 57/2^+$
902.8	0.7	–	E2	9161	$65/2^+ \to 61/2^+$
136.1	5.8	0.46(5)	M1	141	$7/2^+ \to 5/2^+$
193.8	15.7	0.56(5)	M1	499	$11/2^+ \to 9/2^+$
357.6	4.9	0.91(11)	E2	499	$11/2^+ \to 7/2^+$
244.3	7.7	–	M1	955	$15/2^+ \to 13/2^+$
436.3	3.5	–	E2	955	$15/2^+ \to 11/2^+$
455.9	7.5	1.17(11)	E2	955	$15/2^+ \to 11/2^+$
281.1	3.5	–	M1	1478	$19/2^+ \to 17/2^+$
523.5	9.0	0.78(11)	E2	1478	$19/2^+ \to 15/2^+$
308.2	2.5	–	M1	2048	$23/2^+ \to 21/2^+$
569.7	8.0	0.90(9)	E2	2048	$23/2^+ \to 19/2^+$
317.7	2.5	–	M1	2612	$27/2^+ \to 25/2^+$
564.0	4.8	1.10(11)	E2	2612	$27/2^+ \to 23/2^+$
431.1	2.8	–	E2	3043	$31/2^+ \to 27/2^+$
		[514]$9/2^- \otimes$ [AE] band			
554.8	11.8	1.04(9)	E2	2545	$27/2^+ \to 23/2^+$
203.1	5.16	0.60(7)	M1	2968	$31/2^+ \to 29/2^+$

(*continued on next page*)

Table 1 (*continued*)

Energy[a] E_γ (keV)	Intensity[b] I_γ (rel.)	R_{DCO}[c] $I_\gamma(25°)/I_\gamma(90°)$	Multip.	Excitation E_i (keV)	Assignment $J_i^\pi \to J_f^\pi$
423.4	5.8	0.95(11)	E2	2968	$31/2^+ \to 27/2^+$
429.7	3.2	–	E2	2968	$31/2^+ \to 27/2^+$
509.8	10.5	–[d]	E2	2968	$31/2^+ \to 27/2^+$
235.6	11.8	0.49(7)	M1	3437	$35/2^+ \to 33/2^+$
468.2	6.8	0.89(11	E2	3437	$35/2^+ \to 31/2^+$
479.8	8.0	1.05(11)	E2	3437	$35/2^+ \to 31/2^+$
275.2	3.5	0.51(7)	M1	3981	$39/2^+ \to 37/2^+$
544.6	14	1.20(11)	E2	3981	$39/2^+ \to 35/2^+$
562.5	2.4	–[d]	E2	3981	$39/2^+ \to 35/2^+$
309.1	7.5	0.64(8)	M1	4579	$43/2^+ \to 41/2^+$
598.5	13	0.97(9)	E2	4579	$43/2^+ \to 39/2^+$
609.3	6.3	1.05(11)	E2	4579	$43/2^+ \to 39/2^+$
331.9	10.8	0.56(8)	M1	5221	$47/2^+ \to 45/2^+$
641.4	12.3	1.06(9)	E2	5221	$47/2^+ \to 43/2^+$
360.1	7.9	0.81(11)	M1	5900	$51/2^+ \to 49/2^+$
679.2	8.6	0.92(9)	E2	5900	$51/2^+ \to 47/2^+$
395.8	6.4	0.62(8)	M1	6632	$55/2^+ \to 53/2^+$
732.9	6.8	1.25(12)	E2	6632	$55/2^+ \to 51/2^+$
442.0	1.5	–	M1	7439	$59/2^+ \to 57/2^+$
806.9	5.5	0.92(11)	E2	7439	$59/2^+ \to 55/2^+$
493.2	2.6	–	M1	8331	$63/2^+ \to 61/2^+$
891.7	5.0	0.94(11)	E2	8331	$63/2^+ \to 59/2^+$
977.9	3.7	–	E2	9308	$67/2^+ \to 63/2^+$
1058.4	3.1	–	E2	10367	$71/2^+ \to 67/2^+$
1129.7	1.2	–	E2	11497	$75/2^+ \to 71/2^+$
1182.0	0.4	–	E2	12679	$79/2^+ \to 75/2^+$
220.2	1.5	–	M1	2765	$29/2^+ \to 27/2^+$
598.2	4.2	0.97(11)	E2	2765	$29/2^+ \to 25/2^+$
244.1	8.2	0.48(7)	M1	3201	$33/2^+ \to 31/2^+$
435.7	6.0	–[d]	E2	3201	$33/2^+ \to 29/2^+$
470.6	0.8	0.90(18)	E2	3201	$33/2^+ \to 29/2^+$
268.6	6.2	0.47(6)	M1	3705	$37/2^+ \to 35/2^+$
288.8	6.0	0.72(1)	M1	4270	$41/2^+ \to 39/2^+$
299.8	5.4	0.58(7)	M1	4270	$41/2^+ \to 39/2^+$
564.8	1.7	–	E2	4270	$41/2^+ \to 37/2^+$
587.5	5.2	–[d]	E2	4270	$41/2^+ \to 37/2^+$
309.4	12.6	0.64(8)	M1	4889	$45/2^+ \to 43/2^+$
618.5	12.5	0.90(11)	E2	4889	$45/2^+ \to 41/2^+$
318.6	10.3	0.68(9)	M1	5539	$49/2^+ \to 47/2^+$
651.1	12.2	1.16(12)	E2	5539	$49/2^+ \to 45/2^+$
336.0	7.9	0.56(7)	M1	6236	$53/2^+ \to 51/2^+$
696.7	10.9	1.21(15)	E2	6236	$53/2^+ \to 49/2^+$
365.9	3.9	0.69(1)	M1	6998	$57/2^+ \to 55/2^+$
761.4	9.3	1.02(10)	E2	6998	$57/2^+ \to 53/2^+$
398.6	4.5	0.55(8)	M1	7837	$61/2^+ \to 59/2^+$
839.50	8.9	0.98(11)	E2	7837	$61/2^+ \to 57/2^+$
917.2	4.4	1.25(15)	E2	8755	$65/2^+ \to 61/2^+$
987.9	3.3	1.14(16)	E2	9742	$69/2^+ \to 65/2^+$

(*continued*)

Table 1 (*continued*)

Energy[a] E_γ (keV)	Intensity[b] I_γ (rel.)	R_{DCO}[c] $I_\gamma(25°)/I_\gamma(90°)$	Multip.	Excitation E_i (keV)	Assignment $J_i^\pi \to J_f^\pi$
1051.2	2.4	–	E2	10794	$73/2^+ \to 69/2^+$
1105.4	1.5	–	E2	11899	$77/2^+ \to 73/2^+$
1142.2	0.9	–	E2	13041	$81/2^+ \to 77/2^+$
1158.5	0.5	–	E2	14200	$85/2^+ \to 81/2^+$
		N1 band			
715.8	1.4	–	E2	5861	$(49/2^-) \to 45/2^-$
781.3	1.0	–	E2	6642	$(53/2^-) \to (49/2^-)$
824.8	0.9	–	E2	7467	$(57/2^-) \to (53/2^-)$
869.7	0.6	–	E2	8337	$(61/2^-) \to (57/2^-)$
928.3	0.3	–	E2	9265	$(65/2^-) \to (61/2^-)$
		N2 band			
687.2	1.6	–	E2	6081	$51/2^+ \to 47/2^+$
755.0	4.5	1.01(9)	E2	6081	$51/2^+ \to 47/2^+$
393.4	0.9	–	M1	6842	$55/2^+ \to 53/2^+$
761.0	1.42	1.10(11)	E2	6842	$55/2^+ \to 51/2^+$
437.4	1.8	–	M1	7678	$59/2^+ \to 57/2^+$
836.0	2.5	1.04(12)	E2	7678	$59/2^+ \to 55/2^+$
470.4	0.46	–	M1	8585	$63/2^+ \to 61/2^+$
907.0	2.7	1.12(15)	E2	8585	$63/2^+ \to 59/2^+$
960.0	2.6	1.20(15)	E2	9545	$67/2^+ \to 63/2^+$
1002.0	1.5	1.22(17)	E2	10547	$71/2^+ \to 67/2^+$
1036.0	1.4	0.95(15)	E2	11583	$75/2^+ \to 71/2^+$
1061.0	1.2	–	E2	12644	$79/2^+ \to 75/2^+$
		N3 band			
367.6	1.8	–	M1	6449	$53/2^+ \to 51/2^+$
753.0	2.1	1.01(12)	E2	6449	$53/2^+ \to 49/2^+$
398.6	2.1	–	M1	7241	$57/2^+ \to 55/2^+$
792.0	2.2	1.10(14)	E2	7241	$57/2^+ \to 53/2^+$
436.6	0.6	–	M1	8115	$61/2^+ \to 59/2^+$
874.0	2.5	1.20(15)	E2	8115	$61/2^+ \to 57/2^+$
953.0	2.2	1.18(17)	E2	9068	$65/2^+ \to 61/2^+$
1005.0	1.6	–	E2	10073	$69/2^+ \to 65/2^+$
		N4 band			
(840.0)	2.9	–	M1	4575	$41/2^- \to 39/2^-$
598.8	4.1	–	E2	5174	$45/2^- \to 41/2^-$
349.5	1.4	–	M1	5825	$49/2^- \to 47/2^-$
651.2	3.3	–	E2	5825	$49/2^- \to 45/2^-$
373.5	0.5	–	M1	6553	$53/2^- \to 51/2^-$
727.3	2.1	–	E2	6553	$53/2^- \to 49/2^-$
(407.5)	0.3	–	M1	7355	$57/2^- \to 55/2^-$
802.5	1.4	–	E2	7355	$57/2^- \to 53/2^-$
872.2	1.3	–	E2	8227	$61/2^- \to 57/2^-$
928.9	1.2	–	E2	9156	$65/2^- \to 61/2^-$
973.5	1.1	–	E2	10130	$69/2^- \to 65/2^-$
1012.8	0.95	–	E2	11142	$73/2^- \to 69/2^-$
1047.8	0.93	–	E2	12190	$77/2^- \to 73/2^-$

(*continued on next page*)

Table 1 (*continued*)

Energy[a] E_γ (keV)	Intensity[b] I_γ (rel.)	R_{DCO}[c] $I_\gamma(25°)/I_\gamma(90°)$	Multip.	Excitation E_i (keV)	Assignment $J_i^\pi \to J_f^\pi$
		N5 band			
751.2	16.8	1.02(10)	E2	2948	$31/2^- \to 27/2^-$
262.6	5.2	–	M1	3485	$35/2^- \to 33/2^-$
537.6	2.4	–	E2	3485	$35/2^- \to 31/2^-$
695.7	12.2	1.05(9)	E2	3485	$35/2^- \to 31/2^-$
292.9	2.6	0.67(9)	M1	4117	$39/2^- \to 37/2^-$
632.0	5.0	1.00(9)	E2	4117	$39/2^- \to 35/2^-$
320.1	1.7	–	M1	4773	$43/2^- \to 41/2^-$
656.3	4.5	0.90(10)	E2	4773	$43/2^- \to 39/2^-$
702.3	4.2	0.94(11)	E2	5476	$47/2^- \to 43/2^-$
703.0			E2	6179	$51/2^- \to 47/2^-$
352.8	1.2	–	M1	6179	$51/2^- \to 49/2^-$
394.8	0.3	–	M1	6947	$55/2^- \to 53/2^-$
768.6	1.2	0.98(11)	E2	6947	$55/2^- \to 51/2^-$
841.4	1.1	0.83(12)	E2	7789	$59/2^- \to 55/2^-$
903.2	0.55	0.92(15)	E2	8692	$63/2^- \to 59/2^-$
951.2	0.34	0.92(19)	E2	9643	$67/2^- \to 63/2^-$
1001.9	0.16	–	E2	10645	$71/2^- \to 67/2^-$
1039.0	0.11	–	E2	11684	$75/2^- \to 71/2^-$
		N6 band			
275.0	1.1	0.62(9)	M1	3223	$33/2^- \to 31/2^-$
658.1	2.5	–	E2	3223	$33/2^- \to 29/2^-$
687.3	5.2	1.13(12)	E2	3223	$33/2^- \to 29/2^-$
339.0	6.0	0.64(8)	M1	3824	$37/2^- \to 35/2^-$
601.6	6.0	1.10(11)	E2	3824	$37/2^- \to 33/2^-$
628.8	2.5	0.98(11)	E2	3824	$37/2^- \to 33/2^-$
336.6	1.7	–	M1	4454	$41/2^- \to 39/2^-$
629.6	6.2	0.96(11)	E2	4454	$41/2^- \to 37/2^-$
625.0	1.1	–	E2	5116	$45/2^- \to 41/2^-$
662.0	3.0	0.92(12)	E2	5116	$45/2^- \to 41/2^-$
339.8	1.0	–	M1	5787	$49/2^- \to 47/2^-$
670.8	2.6	0.94(12)	E2	5787	$49/2^- \to 45/2^-$
369.4	1.7	–	M1	6508	$53/2^- \to 51/2^-$
721.2	3.9	1.06(12)	E2	6508	$53/2^- \to 49/2^-$
401.4	1.4	–	M1	7288	$57/2^- \to 55/2^-$
780.4	4.1	0.89(12)	E2	7288	$57/2^- \to 53/2^-$
434.0	0.6	–	M1	8128	$61/2^- \to 59/2^-$
839.9	3.8	0.88(11)	E2	8128	$61/2^- \to 57/2^-$
900.1	3.5	0.92(15)	E2	9028	$65/2^- \to 61/2^-$
963.1	2.3	–	E2	9991	$69/2^- \to 65/2^-$
1026.3	1.9	–	E2	11018	$73/2^- \to 69/2^-$
1088.0	1.0	–	E2	12106	$77/2^- \to 73/2^-$
1139.7	0.8	–	E2	13245	$81/2^- \to 77/2^-$
		N7 band			
720.7	0.5	0.63(9)	E1	1770	$19/2^- \to 17/2^+$
386.0	0.96	1.20(15)	E2	2156	$23/2^- \to 19/2^-$

(*continued*)

Table 1 (*continued*)

Energy[a] E_γ (keV)	Intensity[b] I_γ (rel.)	R_{DCO}[c] $I_\gamma(25°)/I_\gamma(90°)$	Multip.	Excitation E_i (keV)	Assignment $J_i^\pi \to J_f^\pi$
568.9	4.6	0.59(7)	E1	2156	$23/2^- \to 21/2^+$
418.3	2.9	0.50(8)	E1	2586	$27/2^- \to 25/2^+$
430.3	8.0	1.04(9)	E2	2586	$27/2^- \to 23/2^-$
481.5	5.4	0.92(9)	E2	3067	$31/2^- \to 27/2^-$
535.1	5.5	1.14(12)	E2	3602	$35/2^- \to 31/2^-$
582.7	4.5	1.02(13)	E2	4185	$39/2^- \to 35/2^-$
615.4	4.9	1.25(15)	E2	4800	$43/2^- \to 39/2^-$
331.0	0.9	–	M1	5447	$47/2^- \to 45/2^-$
646.3	3.6	1.19(16)	E2	5447	$47/2^- \to 43/2^-$
351.5	1.3	–	M1	6138	$51/2^- \to 49/2^-$
691.4	4.0	1.25(16)	E2	6138	$51/2^- \to 47/2^-$
378.9	2.1	–	M1	6887	$55/2^- \to 53/2^-$
748.6	5.5	1.17(15)	E2	6887	$55/2^- \to 51/2^-$
405.9	0.9	–	M1	7694	$59/2^- \to 57/2^-$
807.3	3.2	1.21(15)	E2	7694	$59/2^- \to 55/2^-$
863.1	2.9	–	E2	8557	$63/2^- \to 59/2^-$
918.2	2.3	–	E2	9475	$67/2^- \to 63/2^-$
973.9	2.2	–	E2	10449	$71/2^- \to 67/2^-$
1028.1	1.4	–	E2	11477	$75/2^- \to 71/2^-$
1081.6	1.1	–	E2	12559	$79/2^- \to 75/2^-$
1127.7	0.6	–	E2	13687	$83/2^- \to 79/2^-$
1162.5	0.4	–	E2	14849	$87/2^- \to 83/2^-$
		TSD1 band			
590.7	3.3	1.20(15)	E2	2409	$25/2^+ \to 21/2^+$
384.8	2.0	–	E2	2794	$29/2^+ \to 25/2^+$
445.3	3.5	0.89(17)	E2	2794	$29/2^+ \to 25/2^+$
446.1	2.8	0.89(17)	E2	3240	$33/2^+ \to 29/2^+$
486.5	2.8	0.85(15)	E2	3240	$33/2^+ \to 29/2^+$
525.1	4.6	0.95(12)	E2	3765	$37/2^+ \to 33/2^+$
582.1	5.5	0.89(12)	E2	4347	$41/2^+ \to 37/2^+$
592.7	1.4	–	E2	4347	$41/2^+ \to 37/2^+$
641.3	7.3	1.00(9)	E2	4989	$45/2^+ \to 41/2^+$
696.8	4.9	1.20(14)	E2	5685	$49/2^+ \to 45/2^+$
750.2	4.6	1.12(12)	E2	6436	$53/2^+ \to 49/2^+$
803.3	3.2	0.89(11)	E2	7239	$57/2^+ \to 53/2^+$
855.7	2.8	1.01(11)	E2	8095	$61/2^+ \to 57/2^+$
908.9	2.1	1.14(12)	E2	9003	$65/2^+ \to 61/2^+$
963.0	1.5	0.95(12)	E2	9966	$69/2^+ \to 65/2^+$
1019.3	1.1	0.96(12)	E2	10986	$73/2^+ \to 69/2^+$
1076.3	0.9	–	E2	12062	$77/2^+ \to 73/2^+$
1133.4	0.6	–	E2	13195	$81/2^+ \to 77/2^+$
1189.3	0.4	–	E2	14385	$85/2^+ \to 81/2^+$
1239.3	0.2	–	E2	15624	$89/2^+ \to 85/2^+$
		TSD2 band			
624.4	–	–	E2 + M1	3864	$35/2^+ \to 33/2^+$
538.9	0.58	–	E2	4403	$39/2^+ \to 35/2^+$
638.2	0.24	–	E2 + M1	4403	$39/2^+ \to 37/2^+$

(*continued on next page*)

Table 1 (*continued*)

Energy[a] E_γ (keV)	Intensity[b] I_γ (rel.)	R_{DCO}[c] $I_\gamma(25°)/I_\gamma(90°)$	Multip.	Excitation E_i (keV)	Assignment $J_i^\pi \to J_f^\pi$
598.0	1.0	–	E2	5001	$43/2^+ \to 39/2^+$
654.1	0.27	–	E2 + M1	5001	$43/2^+ \to 41/2^+$
655.1	2.7	–	E2	5656	$47/2^+ \to 43/2^+$
667.9	0.74	–	E2 + M1[e]	5656	$47/2^+ \to 45/2^+$
682.5	0.52	–	E2 + M1[e]	6368	$51/2^+ \to 49/2^+$
711.4	2.6	1.00(9)	E2	6368	$51/2^+ \to 47/2^+$
697.9	0.36	–	E2 + M1	7133	$55/2^+ \to 53/2^+$
765.7	1.7	0.88(14)	E2	7133	$55/2^+ \to 51/2^+$
819.9	1.2	1.05(12)	E2	7953	$59/2^+ \to 55/2^+$
872.1	0.93	0.92(15)	E2	8826	$63/2^+ \to 59/2^+$
926.6	0.79	0.95(17)	E2	9752	$67/2^+ \to 63/2^+$
981.1	0.71	1.13(15)	E2	10733	$71/2^+ \to 67/2^+$
1035.1	0.52	1.14(15)	E2	11768	$75/2^+ \to 71/2^+$
1089.6	0.44	–	E2	12858	$79/2^+ \to 75/2^+$
1151.0	0.27	–	E2	14009	$83/2^+ \to 79/2^+$
1199.8	0.22	–	E2	15209	$87/2^+ \to 83/2^+$
(1253.7)	0.15	–	E2	16462	$(91/2^+ \to 87/2^+)$
			TSD3 band		
661.3	1.5	–	E2	5449	$45/2^+ \to 41/2^+$
(1102.2)	–	–	(E2)	5449	$45/2^+ \to 41/2^+$
706.0	1.6	–	E2	6155	$49/2^+ \to 45/2^+$
(1166.9)	–	–	(E2)	6155	$49/2^+ \to 45/2^+$
748.8	1.7	–	E2	6904	$53/2^+ \to 49/2^+$
(1218.9)	–	–	(E2)	6904	$53/2^+ \to 49/2^+$
798.7	1.9	–	E2	7703	$57/2^+ \to 53/2^+$
849.6	1.8	–	E2	8553	$61/2^+ \to 57/2^+$
904.7	1.5	–	E2	9457	$65/2^+ \to 61/2^+$
957.5	1.3	–	E2	10415	$69/2^+ \to 65/2^+$
1011.1	0.7	–	E2	11426	$73/2^+ \to 69/2^+$
1059.1	0.5	–	E2	12485	$77/2^+ \to 73/2^+$
1107.4	0.3	–	E2	13592	$81/2^+ \to 77/2^+$
			TSD4 band		
624.5	0.6	–	E2		
683.8	1.0	–	E2		
740.7	0.9	–	E2		
798.3	0.8	–	E2		
856.0	0.6	–	E2		
915.6	0.3	–	E2		
975.3	0.2	–	E2		
1037.0	0.1	–	E2		
			TSD5 band		
712.2	0.5	–	E2		
770.2	0.9	–	E2		
828.9	0.8	–	E2		
885.8	0.5	–	E2		
943.7	0.4	–	E2		

(*continued*)

Table 1 (*continued*)

Energy[a] E_γ (keV)	Intensity[b] I_γ (rel.)	R_{DCO}[c] $I_\gamma(25^\circ)/I_\gamma(90^\circ)$	Multip.	Excitation E_i (keV)	Assignment $J_i^\pi \to J_f^\pi$
1002.5	0.3	–	E2		
1063.0	0.1	–	E2		

[a] Uncertainties between 0.1 and 0.8 keV depending on intensity.

[b] Intensities normalized to the 518.8 keV line of the $[514]9/2^-$ band with $I_\gamma = 100$, uncertainties between 8% and 30% depending on intensity.

[c] DCO ratios are normalized to known stretched E2 transitions.

[d] Contamination from a γ-ray line with similar energy.

[e] Mixing of 92.3% E2 + 7.7% M1 was determined from angular correlation analysis [16].

The $[411]1/2^+$ band was only known up to spins $27/2^+$ and $25/2^+$ for the two signature partners, respectively. In this part of the band we add only the 373 keV transition between the two branches. However, above the $27/2^+$ state we add 14 new levels to the $\alpha = -1/2$ sequence up to $83/2^+$. At an excitation energy of around 5 MeV this sequence is perturbed by close-lying levels with spin/parity $43/2^+$, $47/2^+$ and $51/2^+$. In this region several inter-band transitions are observed.

The $\alpha = +1/2$ signature partner of the $[402]5/2^+$ band has been extended by nine states up to spin $65/2^+$. Three new dipole, presumably M1, transitions between the branches have been added. The $[404]7/2^+$ band has also been extended to much higher spin by the addition of eight new levels to each of the two signature branches.

The new sequences labelled N2 and N3 in Fig. 6 are connected by six stretched dipole, presumably M1, inter-band transitions. They form a coupled band decaying into the $47/2^+$ and $49/2^+$ states of the $[404]7/2^+$ band via the 755 and 753 keV stretched quadrupole transitions, respectively. Furthermore, we observe a stretched quadrupole transition of 827 keV from the $55/2^+$ level of the $[404]7/2^+$ band to the N2 sequence. Assuming that these connecting transitions have E2 character (and not M2, which is very unlikely), this fixes positive parity and the spins as shown in Fig. 6 for the bands N2 and N3.

The three-quasiparticle band $[514]9/2^- \otimes [\mathrm{AE}]$ was reported earlier by Schnack-Petersen et al. [3]. We extend this sequence to higher and lower spins and add several new transitions linking it to the $[404]7/2^+$ and $[411]1/2^-$ bands. The $[514]9/2^-$ band was already discussed in detail by Frandsen et al. [5]. The $\alpha = +1/2$ and $-1/2$ signature branches are extended by three transitions to spin $81/2^-$ and by six transitions to $91/2^-$, respectively.

The four new sequences labelled N4, N5, N6 and N7 in Fig. 6 show a peculiar behaviour. In the low-spin region, N5 and N6 are coupled by stretched dipole, presumably M1, transitions, whereas at higher spins N6 and N7 show the same feature and N4 takes over the partnership with N5. Thus, at low spin N5 and N6 form a coupled band, while at high spin N4 and N5 as well as N6 and N7 seem to be coupled. However, we observe no quadrupole transitions between bands N4 and N6 or between bands N5 and N7. The main intensity flow goes through the four sequences as ordered in the level scheme, see also Table 1 and the coincidence spectra displayed in Fig. 4. The sequences N5 and N6 decay into the $[514]9/2^-$ band via the three stretched quadrupole, presumably E2, transitions with energies of 687, 696 and 751 keV. Band N6 decays into the $[541]1/2^-$ band via

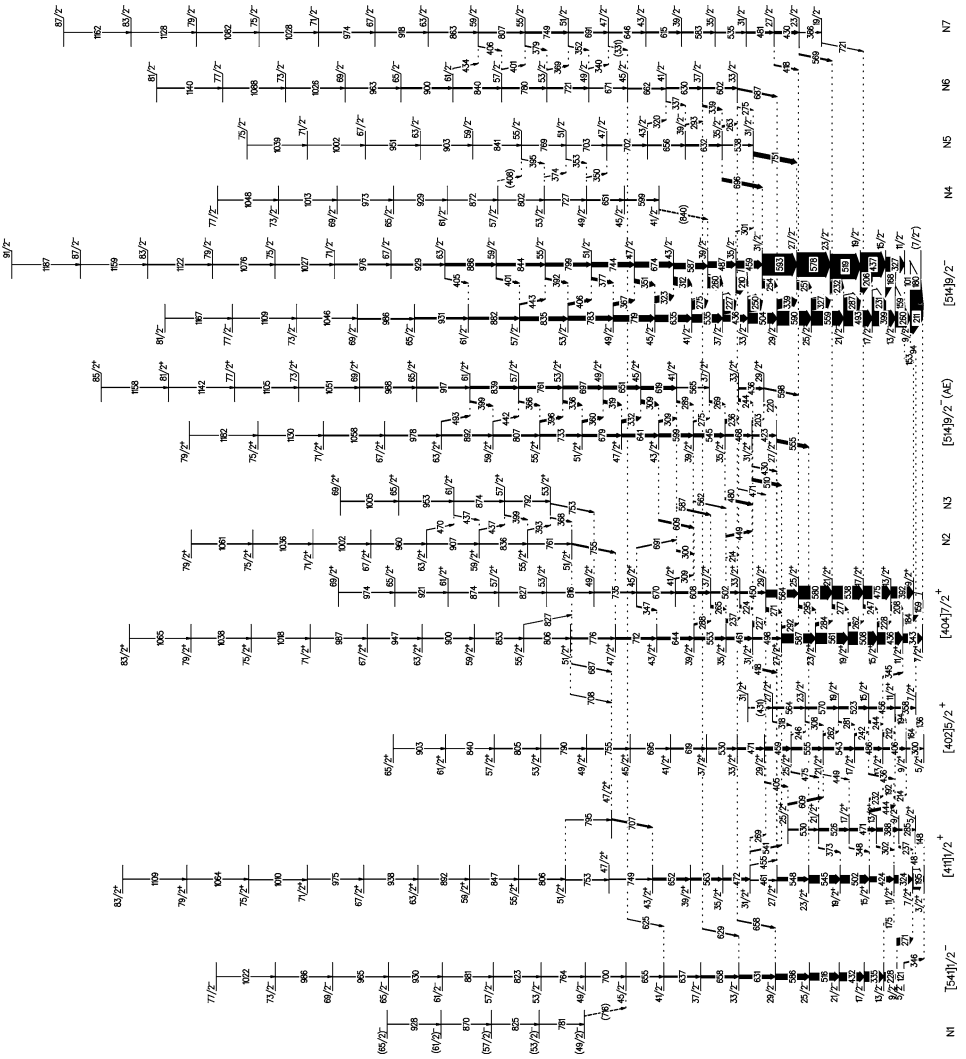

Fig. 6. Partial level scheme of ^{165}Lu, showing the ND bands.

three E2 transitions with energies of 625, 629 and 658 keV. Together with the 301 keV transition from the [514]$9/2^-$ band to N5 and the inter-band M1 transitions between N5 and N6 this decay pattern uniquely determines the spins and parity as shown in Fig. 6. Furthermore, the inter-band M1 transitions between N4 and N5 and between N6 and N7 fix spins and parity of bands N4 and N7. The spin/parity assignment is also compatible with the stretched dipole, presumably E1, character of the three transitions of 418, 569 and 721 keV linking N7 to the [404]$7/2^+$ band. The new band N4 decays also into the [514]$9/2^-$ band. However, those linking transitions could not be established.

A remarkable feature of the level schemes of ^{165}Lu displayed in Figs. 6 and 7 is that so many transitions connecting the various bands exist. This is partly due to the fact that many states of the same spin and parity lie close in energy and substantial mixing can be expected between them. This multitude of connecting transitions uniquely fixes the relative positions of the bands and allows the spin and parity assignments, as explained above.

3. Discussion

The lower-spin members of several bands in the ND level scheme of ^{165}Lu have been known from previous work [3–5]. These band structures are labelled by the previously established Nilsson configurations in Fig. 6. With the exception of the $[541]1/2^-$ band they are coupled bands for which both signature partners are observed.

The behaviour of the previously known band TSD 1 [3] is different from those of the ND bands. The moment of inertia is large over the whole observed frequency range. The new bands labelled TSD 2 to 5 in Fig. 7 have similar dynamic moments of inertia, as can be seen in Fig. 8. They do not show band crossings. The irregularities observed at low frequencies for TSD 1 are due to level mixing with close-lying states. The upbend observed at the highest frequencies might be the onset of a band crossing. The five bands TSD 1 to 5 are associated with the strongly deformed triaxial potential-energy minima found in the calculations, an example of which is given in Fig. 1.

Lifetimes of states within band TSD 1 [14] show that the transition quadrupole moments are substantially larger than for ND states in this mass region. This band is built on an aligned proton $[660]1/2^+$ excitation and is associated with the TSD minimum at $(\epsilon_2, \gamma) = (0.36, 20°)$ seen in Fig. 1 [3,14,16]. Triaxially deformed nuclei may rotate about an axis that does not coincide with one of the principal axes. Therefore, they are expected to show additional modes of excitation compared to axially symmetric nuclei. More than 25 years ago the 'wobbling mode' was predicted for nuclear systems with a stable triaxiality. Wobbling is a unique fingerprint of triaxial deformation. In ^{165}Lu we recently discovered the wobbling mode [16] by an analysis of the decay pattern of bands TSD 2 and 3 into TSD 1. For the decay of TSD 2 into TSD 1 the ratios of reduced E2 transition probabilities for out-of-band to in-band decay, $B(E2)_{out}/B(E2)_{in}$, lie around 0.20. Such unusually large E2 inter-band transition strengths are well explained within the particle-rotor model [25,26] if it is assumed that TSD 1, 2 and 3 form a family of wobbling excitations with phonon quantum numbers $n_w = 0$, 1 and 2.

The bands TSD 4 and 5 are not connected to lower-lying levels, and excitation energies and spins are not known. Therefore, only the dynamic moments of inertia, $J^{(2)}$, can be compared. As seen in Fig. 8, the $J^{(2)}$ values of these two bands are slightly smaller than those of the other TSD bands. However, the similarities suggest that TSD 4 and 5 may also be associated with strongly deformed minima with large triaxiality in the potential-energy surface of ^{165}Lu. The systematic behaviour suggests a spin of $39/2$ or $41/2$ for the lowest-energy level observed for TSD 4 and $45/2$ or $47/2$ for TSD 5. The transition energies of these two bands suggest that they could be signature partners, but no decay between them was found.

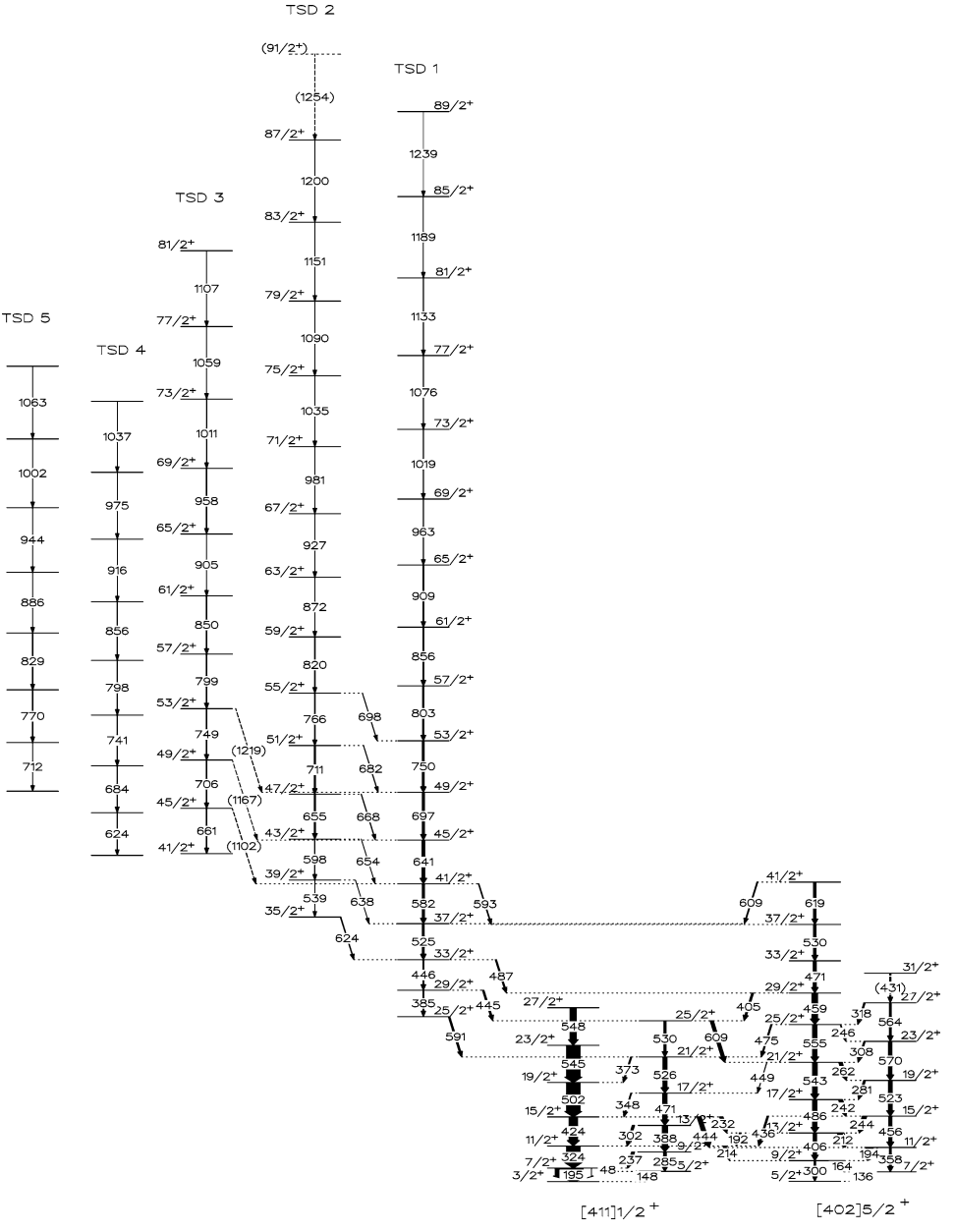

Fig. 7. Partial level scheme of ^{165}Lu, showing the TSD bands and their decay to ND states.

In the following we want to discuss the configuration assignments to the ND structures. In addition to the extension of the previously known bands, the seven new sequences labelled N1 to N7 in Fig. 6 have been established in the present work. As arguments for

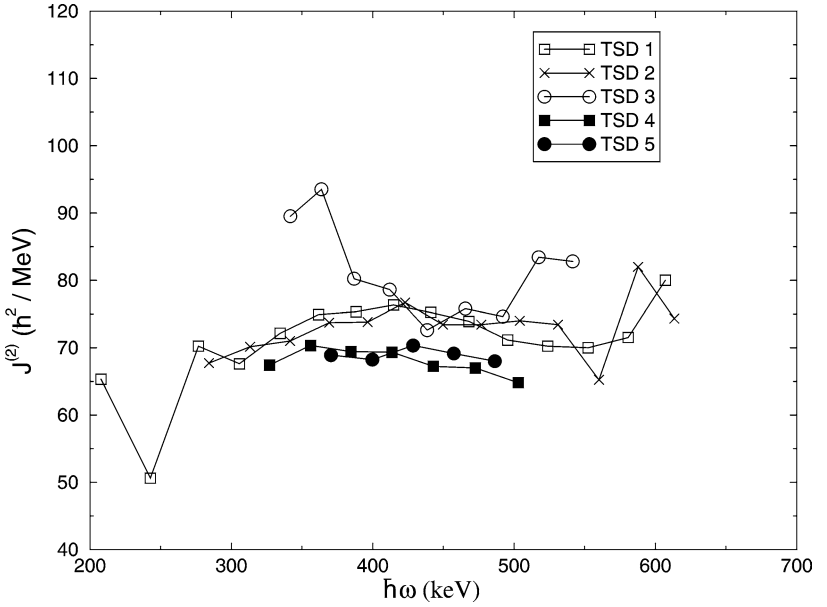

Fig. 8. Dynamic moments of inertia of TSD bands in ^{165}Lu.

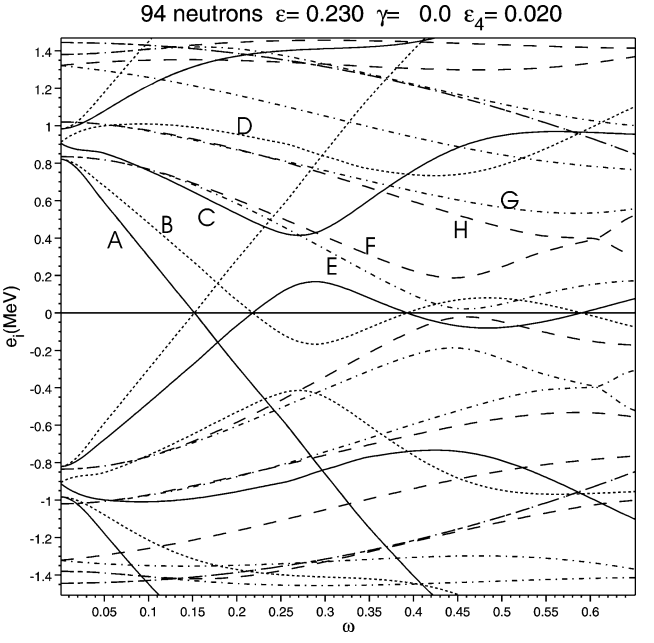

Fig. 9. Quasineutron routhians calculated with the ultimate cranker code [23].

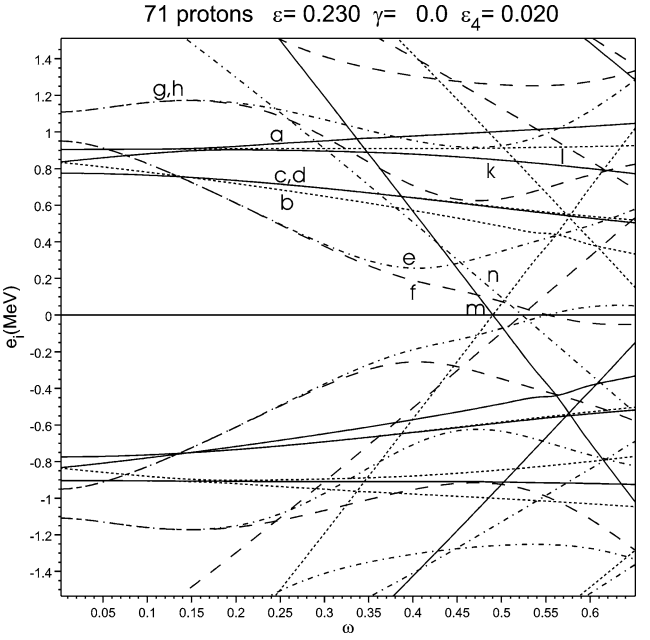

Fig. 10. Quasiproton routhians calculated with the ultimate cranker code [23].

Table 2
Labeling of quasiparticle routhians used in Figs. 9 and 10 and their Nilsson-orbital origins

Quasiprotons		Nilsson	Quasineutrons		Nilsson
$\alpha = +1/2$	$\alpha = -1/2$	orbital	$\alpha = +1/2$	$\alpha = -1/2$	orbital
a	b	$[411]1/2^+$	A	B	$[642]5/2^+$
c	d	$[404]7/2^+$	C	D	$[651]3/2^+$
e	f	$[514]9/2^-$	E	F	$[523]5/2^-$
g	h	$[523]7/2^-$	G	H	$[521]3/2^-$
k	l	$[402]5/2^+$			

configuration assignments to states at higher spins in these bands and to the new bands we are using mainly the observed excitation energies, alignment frequencies and aligned angular momenta in comparison to cranked-shell-model (CSM) calculations. Figs. 9 and 10 show the quasineutron and quasiproton routhians, respectively, calculated with the UC code [23]. According to the CSM convention the routhians are labelled alphabetically [30]. The Nilsson orbitals from which these routhians originate are listed in Table 2.

The experimental excitation energies, relative to a common rotational reference, for the ND bands with positive and negative parity are displayed in Figs. 11 and 12, respectively. As can be seen, many states with the same spin and parity lie very close in energy. This results in level mixing and explains the occurrence of so many inter-band transitions in the level scheme.

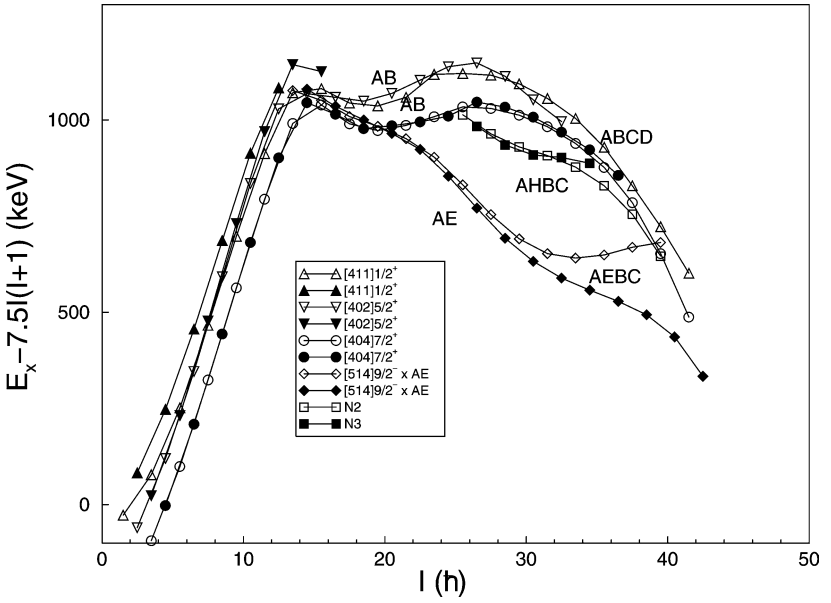

Fig. 11. Experimental excitation energies relative to a rigid-rotor reference core of the positive-parity bands in ^{165}Lu.

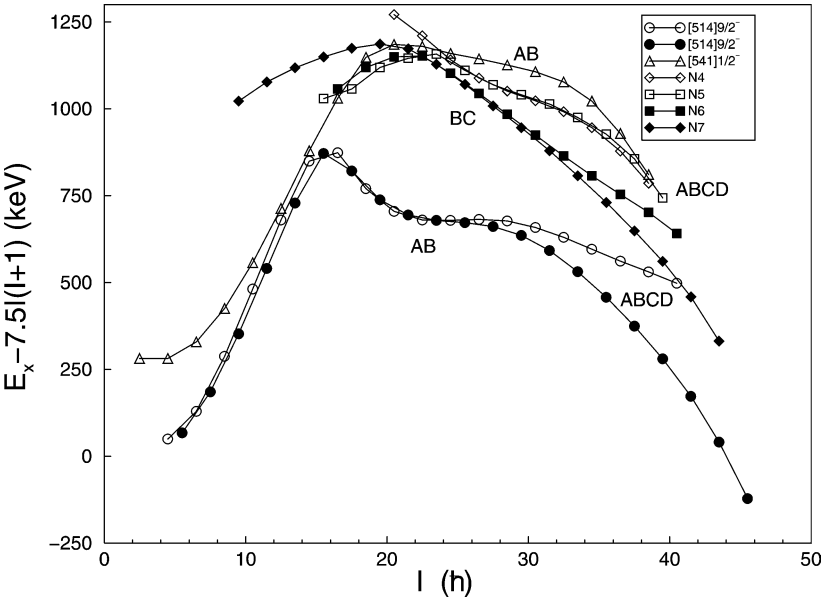

Fig. 12. Experimental excitation energies relative to a rigid-rotor reference core of the negative-parity bands in ^{165}Lu.

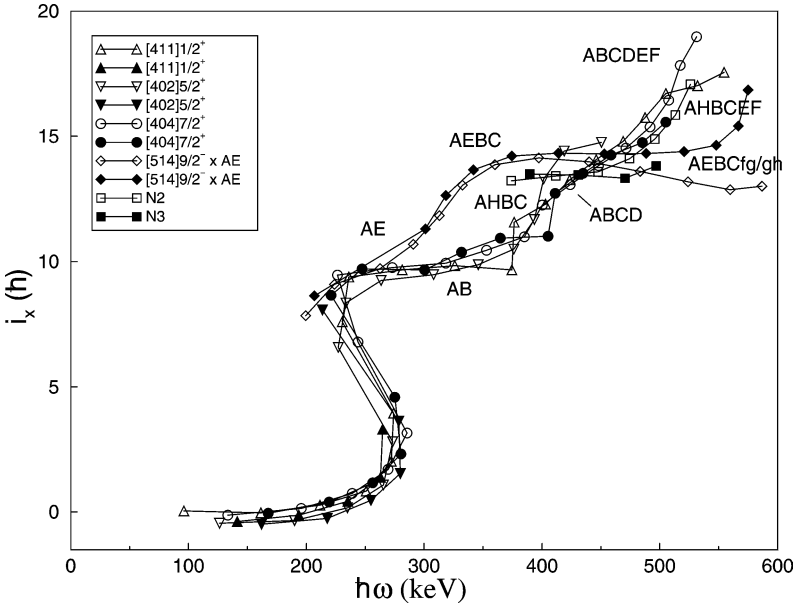

Fig. 13. Experimental alignments of the positive-parity bands in ^{165}Lu (reference core: $J_0 = 30\hbar^2$ MeV^{-1}, $J_1 = 40\hbar^4$ MeV^{-3}).

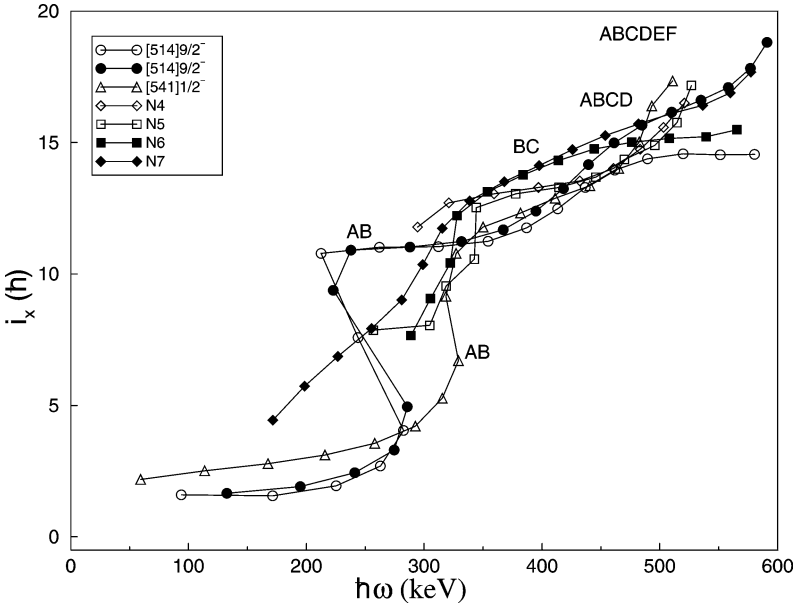

Fig. 14. Experimental alignments of the negative-parity bands in ^{165}Lu (reference core: $J_0 = 30\hbar^2$ MeV^{-1}, $J_1 = 40\hbar^4$ MeV^{-3}).

The aligned angular momenta for the positive- and negative-parity states are compared in Figs. 13 and 14, respectively. The alignment at lowest rotational frequency occurs for most bands at $\hbar\omega = 0.25$ MeV with an alignment gain of about $10\hbar$. An exception is the $[541]1/2^-$ band where the first alignment is delayed to 0.32 MeV. A similar delay has been observed for this configuration in other nuclei of this mass region. The reason for the delayed crossing is not fully understood. Several approaches have been used to reproduce the observed crossing frequencies and alignments. The deformation of the odd-mass nuclei increases if the $[541]1/2^-$ orbital is populated. However, CSM calculations [31] show that the larger deformation and a variation of pairing within reasonable limits can only partly account for the observations. In addition, proton–neutron residual interactions between the $h_{9/2}$ protons and the $i_{13/2}$ neutrons have been proposed. They lead to a configuration mixing in the band-crossing region and can result in a shift of the crossing frequency [32].

Comparison to the UC calculations shows that the first alignment is due to the decoupling of a pair of quasineutrons (AB) of $i_{13/2}$ origin. This explains the large alignment gain of about $10\hbar$. The alignments of the next pairs of quasineutrons of $i_{13/2}$ origin, BC and CD, occur at higher frequencies, around 0.31 and 0.40 MeV, respectively. They show a smaller alignment gain of about $4.5\hbar$. The CD alignment and that of the first natural-parity quasineutron pair (EF) occur at similar frequencies. We will now discuss the configuration assignments to the band structures shown in Fig. 6, proceeding from left to right.

The $[541]1/2^-$ band was already mentioned above to show a higher AB alignment frequency than the other configurations. As a result of the present work, the alignment of the next quasineutron pair, CD, is observed, see Fig. 14. It lies at somewhat higher frequency than in the other bands and is probably followed immediately by the EF alignment. From low to high spins, this band has the configuration $[541]1/2^-$, $[541]1/2^- \otimes [\mathrm{AB}]$, $[541]1/2^- \otimes [\mathrm{ABCD}]$ and $[541]1/2^- \otimes [\mathrm{ABCDEF}]$.

The $[411]1/2^+$ band was previously observed into the first band-crossing region [3]. The new levels of the $\alpha = -1/2$ sequence established in the present work allow to determine the alignment gain of $10\hbar$. Thus, the $[411]1/2^+$ band is crossed by the $[411]1/2^+ \otimes [\mathrm{AB}]$ configuration. At higher spins the CD alignment is observed and the band goes over into the $[411]1/2^+ \otimes [\mathrm{ABCD}]$ configuration. The $[411]1/2^+ \otimes [\mathrm{AB}]$ band is somewhat perturbed at medium spins because levels with spins $43/2^+$, $47/2^+$ and $51/2^+$ lie close in energy and mix. A number of cross-band transitions are observed in this spin region.

The $\alpha = +1/2$ signature branch of the $[402]5/2^+$ band is now extended well above the AB crossing into the CD alignment, see Fig. 13. Thus, this band has the configuration $[402]5/2^+$, $[402]5/2^+ \otimes [\mathrm{AB}]$ and $[402]5/2^+ \otimes [\mathrm{ABCD}]$ following it from low to high rotational frequency. Only the $\alpha = +1/2$ signature partner is observed above the first quasineutron alignment. New data for neighbouring ^{167}Lu [33] also show only one signature branch up to high spins for the $[411]1/2^+$ and $[402]5/2^+$ bands. Possibly the alignment causes a signature splitting that results in a smaller feeding of the unfavoured sequences.

For the $[404]7/2^+$ band the AB quasineutron alignment was already known previously [3]. Here, we observe this configuration through the CD band crossing and into the onset of a further alignment at the highest frequencies, possibly of EF quasineutrons or a pair of quasiprotons. With increasing spin the band changes from $[404]7/2^+$, $[404]7/2^+ \otimes [\mathrm{AB}]$

and $[404]7/2^+ \otimes [ABCD]$ into a seven-quasiparticle configuration. The nature of the seven-quasiparticle configuration will be discussed below.

The two new sequences N2 and N3, see Fig. 6, form a coupled band with positive parity that decays into the $[404]7/2^+ \otimes [AB]$ configuration from the $51/2^+$ and $53/2^+$ levels. The decay pattern demonstrates an interaction between the bands at these spins. A continuation to lower spins is not observed. As can be seen in Fig. 13, its alignment is high, initially $13.8\hbar$, and shows a further increase at the highest observed rotational frequencies. The initial alignment is slightly lower than that of the previously known [3] positive-parity $[514]9/2^- \otimes [AE]$ band after it has gone through the BC crossing and has become the $[514]9/2^- \otimes [AEBC]$ configuration. On the other hand, the excitation energy of the new band is higher and the signature splitting, observed in both the N2, N3 bands and in the $[514]9/2^- \otimes [AE]$ bands, is opposite. These experimental properties and comparison to the calculated routhians, see Fig. 9, suggest that the most likely configuration of bands N2 and N3 is $[514]9/2^- \otimes [AHBC]$. At the highest frequencies this probably goes over into a seven-quasiparticle configuration. We will comment on the nature of the seven-quasiparticle configuration in the following paragraph.

For the previously known band [3] labelled $[514]9/2^- \otimes [AE]$ in Fig. 6, we have just mentioned that it becomes the $[514]9/2^- \otimes [AEBC]$ configuration at higher frequencies. Inspection of Fig. 13 shows that it does not upbend at a frequency of about 0.5 MeV, as the $[514]9/2^- \otimes [AHBC]$ band N2, N3 does. This can be explained if the alignment gain observed at $\hbar\omega = 0.52$ MeV in the N2, N3 band is caused by the EF quasineutrons which is blocked in the $[514]9/2^- \otimes [AEBC]$ configuration. The onset of an upbend seen in the $[514]9/2^- \otimes [AEBC]$ band at still higher frequencies, $\hbar\omega \approx 0.56$ MeV, might then be due to quasiproton alignment. Inspection of the proton quasiparticle diagram, see Fig. 10, shows that only the ef and gh proton pairs provide sufficient alignment gain. As the orbital e is blocked in this configuration involving the $[514]9/2^-$ proton, the aligning proton pair is most likely fg or gh.

In view of these arguments, let us return to the suggested crossing with a seven-quasiparticle configuration at the highest spins in the $[404]7/2^+ \otimes [ABCD]$ band mentioned above. The alignment frequency of 0.52 MeV appears to be the same as for the seven-quasiparticle configuration $[514]9/2^- \otimes [AHBCEF]$ just discussed. Thus, at the highest observed frequencies, the $[404]7/2^+$ band has probably the $[404]7/2^+ \otimes [ABCDEF]$ configuration and the alignment of a pair of quasiprotons might occur at even higher frequencies.

The remaining bands to be discussed, $[514]9/2^-$ and N4 to N7, have negative parity. The previously known [4] $[514]9/2^-$ band shows the AB crossing at a frequency of 0.25 MeV. At higher frequencies, the $[514]9/2^- \otimes [AB]$ configuration is crossed by the band with an additional $i_{13/2}$ quasineutron alignment, $[514]9/2^- \otimes [ABCD]$. In this frequency range the two signatures split and the $\alpha = -1/2$ branch shows a larger alignment.

From the plot of excitation energy versus spin shown in Fig. 12 it is clear that bands N4, N5 and bands N6, N7 form pairs of signature-partner bands at spins above $45/2$. In the region $47/2$ to $61/2$ bands N6 and N7 show mutual cross-band transitions, and between $I = 47/2$ and $57/2$ cross-band transitions are found between bands N4 and N5. At lower spin the bands apparently form pairs differently. Band N6 interchanges character with band N4, as mutual interband transitions between N5 and N6 occur below $I = 45/2$ where bands

N5 and N6 indeed come close in excitation energy as partners. The two lowest states in N4 may then be the real low spin extension of the high spin structure of band N6 although cross-band connections to N7 are missing. In fact, the lower part of N7 is possibly of a different structure.

The structure at low spin may also be traced in the decay-out properties of these bands. For N5 and N6 the observed decay by stretched E2 transitions to the $[514]9/2^-$ band in the region of the AB crossing, together with the alignment behaviour suggest that these bands form the extension of the $[514]9/2^-$ band to higher spin (yrare band). It experiences an alignment at the BC crossing frequency, but no alignment at the CD frequency, consistent with blocking. Thus, we assign the configuration $[514]9/2^- \otimes [\mathrm{BC}]$ to N5, N6 going into N5, N4 at $I = 49/2^-$. The alignment gain at $\hbar\omega \sim 0.5$ MeV may be caused the EF neutrons.

Bands N6 and N7 show a larger alignment than N4 and N5 in the region above $I = 45/2$ where they obviously form a pair of signature partners. They come closer to the yrast band $[514]9/2^- \otimes [\mathrm{AB}]$ with increasing spin than bands N4, N5. They also show no CD crossing, so most likely the C quasineutron is involved in the configuration. We expect that negative-parity bands built on the lowest positive-parity configurations coupled to the AE quasineutrons, with the BC neutrons also aligned, may be found. Thus, the most likely configuration is $[404]7/2^+ \otimes [\mathrm{AE}]$ going into $[404]7/2^+ \otimes [\mathrm{AEBC}]$. This interpretation is supported by a comparison of the difference in routhian energies between N6, N7 and $[404]7/2^+ \otimes [\mathrm{AB}]$ (0.23 MeV) with the corresponding difference between $[514]9/2^- \otimes [\mathrm{AE}]$ and $[514]9/2^- \otimes [\mathrm{AB}]$ (0.24 MeV) at a rotational frequency of 0.3 MeV. The lower-spin part of N7 shows a gradual alignment gain, quite different from any of the other observed bands which resembles that observed for the unfavoured partner of the $[541]1/2^-$ orbital [31]. However, the E1 decay to the $[404]7/2^+$ orbital could also point to an octupole enhancement in the $[404]7/2^+ \otimes [\mathrm{AE}]$ configuration at the lower spins.

With the above interpretations, N5 is the only band which has the same structure in the entire observed spin range. It is going from $[514]9/2^-$ into the configuration $[514]9/2^- \otimes [\mathrm{BC}]$ and possibly into $[514]9/2^- \otimes [\mathrm{BCEF}]$. In the spin region where all the bands come quite close in energy and interactions occur, N6 changes from $[514]9/2^- \otimes [\mathrm{BC}]$ at high spin to $[404]7/2^+ \otimes [\mathrm{AE}]$ at lower spin, N4 probably from $[404]7/2^+ \otimes [\mathrm{AE}]$ at high spin to $[514]9/2^- \otimes [\mathrm{BC}]$ at lower spin and N7 either from the unfavoured $[541]1/2^-$ signature partner or from an octupole vibrational excitation built on the $[404]7/2^+$ band at low spin into the $[404]7/2^+ \otimes [\mathrm{AE}]$ configuration. It is, however, strange in such a scenario that no stretched E2 transitions are observed between N4 and N6 in the region of interaction around spin 45/2. To our knowledge this is the first time that such a configuration exchange is observed between bands. One could note though, that the closeness of the $[541]1/2^-$ band with N6 presumably causes an interaction in the same region, as documented by the decay via stretched E2 transitions from N6 to states of the $[541]1/2^-$ band. The decay pattern in the mixed region may therefore be complicated by a three-band mixing scenario.

4. Summary

In summary, high-spin γ-ray spectroscopy has been performed on ^{165}Lu with the EUROBALL spectrometer array. The energy level scheme has been considerably extended.

Nine new bands were found and the previously known bands have been observed to much higher spins. In this nucleus ND shapes coexist with TSD shapes. Three of the TSD bands form a family of wobbling excitations. Wobbling is a unique fingerprint of nuclear triaxiality.

Configuration assignments have been made to the ND bands for which spin and parity assignments could be made. The band structures can be followed through several band crossings up to seven quasi-particle configurations. The $[514]9/2^-$ band with its successive alignments of the AB and CD pairs of neutrons is yrast in the full spin range up to $91/2^-$. The lowest configuration with positive parity, $[404]7/2^+$, is crossed already around spin 20 by the band with the configuration $[514]9/2^- \otimes [\mathrm{AE}]$ in which the two quasineutrons form a pair of negative-parity bands. Above spin 25 also the second-lowest band of positive parity has a similar structure, involving the $[514]9/2^-$ orbital coupled to the AH neutrons.

An interesting new phenomenon is the observed exchange of configuration between the two bands N4 and N6 due to mixing in the intermediate spin range. At low spin N5 and N6 form a strongly coupled band to which we assign $[514]9/2^- \otimes [\mathrm{BC}]$ and at higher spin N5 and N4 have probably changed into that configuration. This exchange of character is clearly supported by an exchange of partnership documented by the occurrence of cross-band M1 transitions. However, no stretched E2 transitions are observed to connect the interacting bands.

Acknowledgements

This work was supported by BMBF, Germany (Contract No. 06 BN 907), by the Danish Science Foundation, by the Polish State Committee for Scientific Research (KBN Grant No. 2 P03B 11822) and by the EU (Contract No. HPRICT-1999-00078).

References

[1] W. Schmitz, C.X. Yang, H. Hübel, A.P. Byrne, R. Müßeler, N. Singh, K.H. Maier, A. Kuhnert, R. Wyss, Nucl. Phys. A 539 (1992) 112.
[2] W. Schmitz, H. Hübel, C.X. Yang, G. Baldsiefen, U. Birkental, G. Frölingsdorf, D. Mehta, R. Müßeler, M. Neffgen, P. Willsau, G.B. Hagemann, A. Maj, D. Müller, J. Nyberg, M. Piiparinen, A. Virtanen, R. Wyss, Phys. Lett. B 303 (1993) 230.
[3] H. Schnack-Petersen, R. Bengtsson, R.A. Bark, P. Bosetti, A. Brockstedt, H. Carlsson, L.P. Ekström, G.B. Hagemann, B. Herskind, F. Ingebretsen, H.J. Jensen, S. Leoni, A. Nordlund, H. Ryde, P.O. Tjøm, C.X. Yang, Nucl. Phys. A 594 (1995) 175.
[4] S. Jonsson, J. Lyttkens, L. Carlen, N. Roy, H. Ryde, W. Walus, L. Kownacki, G.B. Hagemann, B. Herskind, J.D. Garrett, P.O. Tjøm, Nucl. Phys. A 422 (1984) 397.
[5] P. Frandsen, R. Chapman, J.D. Garrett, G.B. Hagemann, B. Herskind, C.-H. Yu, K. Schiffer, D. Clarke, F. Khazaie, J.C. Lisle, J.N. Mo, L. Carlen, P. Eckström, H. Ryde, Nucl. Phys. A 489 (1988) 508.
[6] C.X. Yang, X.G. Wu, H. Zheng, X.A. Liu, Y.S. Chen, C.W. Shen, Y.J. Ma, J.B. Lu, S. Wen, G.S. Li, S.G. Li, G.J. Yuan, P.K. Weng, Y.Z. Liu, Eur. Phys. J. A 1 (1998) 237.
[7] S. Törmänen, S.W. Ødegård, G.B. Hagemann, A. Harsmann, M. Bergström, R.A. Bark, B. Herskind, G. Sletten, P.O. Tjøm, A. Görgen, H. Hübel, B. Aengenvoort, U.J. van Severen, C. Fahlander, D. Napoli,

S. Lenzi, C. Petrache, C. Ur, H.J. Jensen, H. Ryde, R. Bengtsson, A. Bracco, S. Frattini, R. Chapman, D.M. Cullen, S.L. King, Phys. Lett. B 454 (1999) 8.

[8] J. Domscheit, S. Törmänen, B. Aengenvoort, H. Hübel, R.A. Bark, M. Bergström, A. Bracco, R. Chapman, D.M. Cullen, C. Fahlander, S. Frattini, A. Görgen, G.B. Hagemann, A. Harsmann, B. Herskind, H.J. Jensen, S.L. King, S. Lenzi, S.W. Ødegård, C.M. Petrache, H. Ryde, U.J. van Severen, G. Sletten, P.O. Tjøm, C. Ur, Nucl. Phys. A 660 (1999) 381.

[9] H. Amro, P.G. Varmette, W.C. Ma, B. Herskind, G.B. Hagemann, G. Sletten, R.V.F. Janssens, M. Bergström, A. Bracco, M. Carpenter, J. Domscheit, S. Frattini, D.J. Hartley, H. Hübel, T.L. Khoo, F. Kondev, T. Lauritsen, C.J. Lister, B. Million, S.W. Ødegård, R.B. Piercey, L.L. Riedinger, K.A. Schmidt, S. Siem, I. Wiedenhöver, J.N. Wilson, J.A. Winger, Phys. Lett. B 506 (2001) 39.

[10] S.W. Ødegård, G.B. Hagemann, D.R. Jensen, M. Bergström, B. Herskind, G. Sletten, S. Törmänen, J.N. Wilson, P.O. Tjøm, I. Hamamoto, K. Spohr, H. Hübel, A. Görgen, G. Schönwasser, A. Bracco, S. Leoni, A. Maj, C.M. Petrache, P. Bednarczyk, D. Curien, Phys. Rev. Lett. 86 (2001) 5866.

[11] D.R. Jensen, G.B. Hagemann, I. Hamamoto, S.W. Ødegård, B. Herskind, G. Sletten, J.N. Wilson, K. Spohr, H. Hübel, P. Bringel, A. Neußer, G. Schönwaßer, A.K. Singh, W.C. Ma, H. Amro, A. Bracco, S. Leoni, G. Benzoni, A. Maj, C.M. Petrache, G. Lo Bianco, P. Bednarczyk, D. Curien, Phys. Rev. Lett. 89 (2002) 142503.

[12] D.R. Jensen, G.B. Hagemann, I. Hamamoto, S.W. Ødegård, M. Bergström, B. Herskind, G. Sletten, S. Törmänen, J.N. Wilson, P.O. Tjøm, K. Spohr, H. Hübel, A. Görgen, G. Schönwasser, A. Bracco, S. Leoni, A. Maj, C.M. Petrache, P. Bednarczyk, D. Curien, Nucl. Phys. A 703 (2002) 3.

[13] G. Schönwaßer, H. Hübel, G.B. Hagemann, J. Domscheit, A. Görgen, B. Herskind, G. Sletten, D.R. Napoli, C. Rossi-Alvarez, D. Bazzacco, R. Bengtsson, P.O. Tjöm, S.W. Ødegård, Eur. Phys. J. A 13 (2002) 291.

[14] G. Schönwaßer, H. Hübel, G.B. Hagemann, H. Amro, R.M. Clark, M. Cromaz, R.M. Diamond, P. Fallon, B. Herskind, G. Lane, W.C. Ma, A.O. Macchiavelli, S.W. Ødegård, G. Sletten, D. Ward, J.N. Wilson, Eur. Phys. J. A 15 (2002) 435.

[15] A. Görgen, R.M. Clark, M. Cromaz, P. Fallon, G.B. Hagemann, H. Hübel, I.Y. Lee, A.O. Macchiavelli, G. Sletten, D. Ward, R. Bengtsson, preprint.

[16] G. Schönwaßer, H. Hübel, G.B. Hagemann, P. Bednarczyk, G. Benzoni, G. Lo Bianco, A. Bracco, P. Bringel, R. Chapman, D. Curien, J. Domscheit, B. Herskind, D.R. Jensen, S. Leoni, W.C. Ma, A. Maj, A. Neußer, S.W. Ødegård, C.M. Petrache, D. Roßbach, H. Ryde, K.H. Spohr, A.K. Singh, Phys. Lett. B 552 (2003) 9.

[17] A. Neußer, H. Hübel, G.B. Hagemann, S. Bhattacharya, P. Bringel, D. Curien, O. Dorvaux, J. Domscheit, F. Hannachi, D.R. Jensen, A. Lopez-Martens, E. Mergel, N. Nenoff, A.K. Singh, Eur. Phys. J. A 15 (2002) 439.

[18] P. Bringel, H. Hübel, H. Amro, M. Axiotis, D. Bazzacco, S. Bhattacharya, R. Bhowmik, J. Domscheit, G.B. Hagemann, D.R. Jensen, Th. Kröll, S. Lunardi, D.R. Napoli, A. Neußer, S.C. Pancholi, C.M. Petrache, G. Schönwasser, A.K. Singh, C. Ur, Eur. Phys. J. A 16 (2003) 155.

[19] H. Amro, W.C. Ma, G.B. Hagemann, B. Herskind, G. Sletten, J.N. Wilson, D.R. Jensen, J. Thompson, J.A. Winger, P. Fallon, D. Ward, R.M. Diamond, A. Görgen, A.O. Macchiavelli, H. Hübel, J. Domscheit, I. Wiedenhöver, Phys. Lett. B 553 (2003) 197.

[20] M.K. Djongolov, D.J. Hartley, L.L. Riedinger, F.G. Kondev, R.V.F. Janssens, K. Abu Saleem, I. Ahmad, D.L. Balabanski, M.P. Carpenter, P. Chowdhury, D.M. Cullen, M. Danchev, G.D. Dracoulis, H. El-Masri, J. Goon, A. Heinz, R.A. Kaye, T.L. Khoo, T. Lauritsen, C.J. Lister, E.F. Moore, M.A. Riley, D. Seweryniak, I. Shestakova, G. Sletten, P.M. Walker, C. Wheldon, I. Wiedenhöver, O. Zeidan, J.-Y. Zhang, Phys. Lett. B 560 (2003) 24.

[21] I. Ragnarsson, Phys. Rev. Lett. 62 (1989) 2084.

[22] S. Åberg, Nucl. Phys. A 520 (1990) 35c.

[23] T. Bengtsson, Nucl. Phys. A 496 (1989) 56;
T. Bengtsson, Nucl. Phys. A 512 (1990) 124.

[24] A. Bohr, B. Mottelson, Nuclear Structure, vol. 2, Benjamin, New York, 1975.

[25] I. Hamamoto, Phys. Rev. C 65 (2002) 044305.

[26] I. Hamamoto, G.B. Hagemann, Phys. Rev. C 67 (2003) 014319.

[27] J. Simpson, Z. Phys. A 358 (1997) 139.

[28] D.C. Radford, Nucl. Instrum. Methods Phys. Res. A 361 (1995) 297.

[29] M. Cromaz, T.J.M. Symons, G.J. Lane, I.Y. Lee, R.W. MacLeod, Nucl. Instrum. Methods Phys. Res. A 462 (2001) 519.
[30] R. Bengtsson, S. Frauendorf, Nucl. Phys. A 314 (1979) 27.
[31] H.J. Jensen, R.A. Bark, P.O. Tjøm, G.B. Hagemann, I.G. Bearden, H. Carlsson, S. Leoni, T. Lönnroth, W. Reviol, L.L. Riedinger, H. Schnack-Petersen, T. Shizuma, X.Z. Wang, J. Wrzesinski, Nucl. Phys. A 695 (2001) 3.
[32] R.A. Bark, H. Carlsson, S.J. Freeman, G.B. Hagemann, F. Ingebretsen, H.J. Jensen, T. Lönnroth, M.J. Piiparinen, I. Ragnarsson, H. Ryde, H. Schnack-Petersen, P.B. Semmes, P.O. Tjøm, Nucl. Phys. A 630 (1998) 603.
[33] W.C. Ma, private communication.